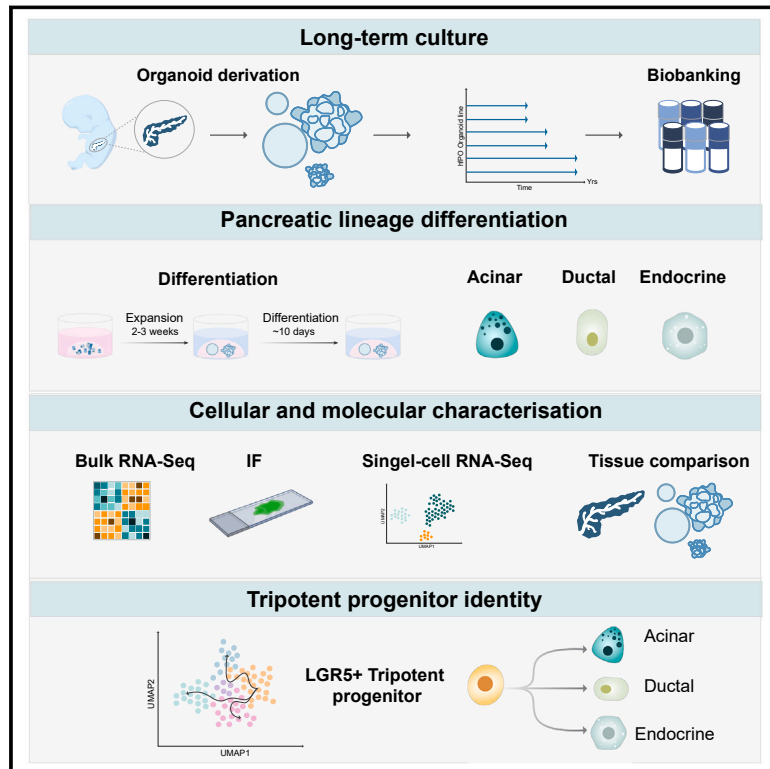


# Long-term *in vitro* expansion of a human fetal pancreas stem cell that generates all three pancreatic cell lineages

## Graphical abstract



## Authors

Amanda Andersson-Rolf, Kelvin Groot, Jeroen Korving, ..., Alexander van Oudenaarden, Johan H. van Es, Hans Clevers

## Correspondence

a.andersson@hubrecht.eu (A.A.-R.), h.clevers@hubrecht.eu (H.C.)

## In brief

Identification of an LGR5 as a marker for a tripotent stem/progenitor cell of the human fetal pancreas. Organoids derived from single LGR5<sup>+</sup> cells are capable of long-term expansion *in vitro* and generation of the three main epithelial cell lineages that make up the mammalian pancreas.

## Highlights

- Human fetal pancreatic organoids (hfPOs) established from 8 to 17 GWs expand long-term
- hfPOs recapitulate the epithelial complexity of human fetal pancreas
- hfPOs generate functional acinar and endocrine cell lineages upon differentiation
- LGR5 marks tripotent stem cells, precursors to all exocrine and endocrine lineages



Article

# Long-term *in vitro* expansion of a human fetal pancreas stem cell that generates all three pancreatic cell lineages

Amanda Andersson-Rolf,<sup>1,2,\*</sup> Kelvin Groot,<sup>1,2,9</sup> Jeroen Korving,<sup>1,2</sup> Harry Begthel,<sup>1,2</sup> Maaïke A.J. Hanegraaf,<sup>3</sup> Michael VanInsberghe,<sup>1,2</sup> Fredrik Salmén,<sup>1,2</sup> Stieneke van den Brink,<sup>1,2</sup> Carmen Lopez-Iglesias,<sup>4</sup> Peter J. Peters,<sup>4</sup> Daniel Krueger,<sup>1,2</sup> Joep Beumer,<sup>6</sup> Maarten H. Geurts,<sup>1,2,5</sup> Anna Alemany,<sup>7</sup> Helmuth Gehart,<sup>8</sup> Françoise Carlotti,<sup>3</sup> Eelco J.P. de Koning,<sup>3</sup> Susana M. Chuva de Sousa Lopes,<sup>7</sup> Alexander van Oudenaarden,<sup>1,2</sup> Johan H. van Es,<sup>1,2</sup> and Hans Clevers<sup>1,2,5,6,10,\*</sup>

<sup>1</sup>Hubrecht Institute, Oncode Institute, Royal Netherlands Academy of Arts and Sciences (KNAW), 3584 CT Utrecht, the Netherlands

<sup>2</sup>University Medical Center Utrecht, 3584 CX Utrecht, the Netherlands

<sup>3</sup>Department of Internal Medicine, Leiden University Medical Center, 2333 ZA Leiden, the Netherlands

<sup>4</sup>The Maastricht Multimodal Molecular Imaging Institute, 6229 ER Maastricht, the Netherlands

<sup>5</sup>Princess Maxima Centre for Pediatric Oncology, 3584 CS Utrecht, the Netherlands

<sup>6</sup>Institute of Human Biology (IHB), Roche Pharma Research and Early Development, Roche innovation Centre, 4070 Basel, Switzerland

<sup>7</sup>Department of Anatomy and Embryology, Leiden University Medical Centre, 2333 ZA Leiden, the Netherlands

<sup>8</sup>ETH Zurich, Institute of Molecular Health Sciences, 8093 Zürich, Schweiz

<sup>9</sup>Present address: Department of Molecular Life Sciences, University of Zürich, 8057 Zürich, Switzerland

<sup>10</sup>Lead contact

\*Correspondence: [a.andersson@hubrecht.eu](mailto:a.andersson@hubrecht.eu) (A.A.-R.), [h.clevers@hubrecht.eu](mailto:h.clevers@hubrecht.eu) (H.C.)

<https://doi.org/10.1016/j.cell.2024.10.044>

## SUMMARY

The mammalian pancreas consists of three epithelial compartments: the acini and ducts of the exocrine pancreas and the endocrine islets of Langerhans. Murine studies indicate that these three compartments derive from a transient, common pancreatic progenitor. Here, we report derivation of 18 human fetal pancreas organoid (hfPO) lines from gestational weeks 8–17 (8–17 GWs) fetal pancreas samples. Four of these lines, derived from 15 to 16 GWs samples, generate acinar-, ductal-, and endocrine-lineage cells while expanding exponentially for >2 years under optimized culture conditions. Single-cell RNA sequencing identifies rare LGR5<sup>+</sup> cells in fetal pancreas and in hfPOs as the root of the developmental hierarchy. These LGR5<sup>+</sup> cells share multiple markers with adult gastrointestinal tract stem cells. Organoids derived from single LGR5<sup>+</sup> organoid-derived cells recapitulate this tripotency *in vitro*. We describe a human fetal tripotent stem/progenitor cell capable of long-term expansion *in vitro* and of generating all three pancreatic cell lineages.

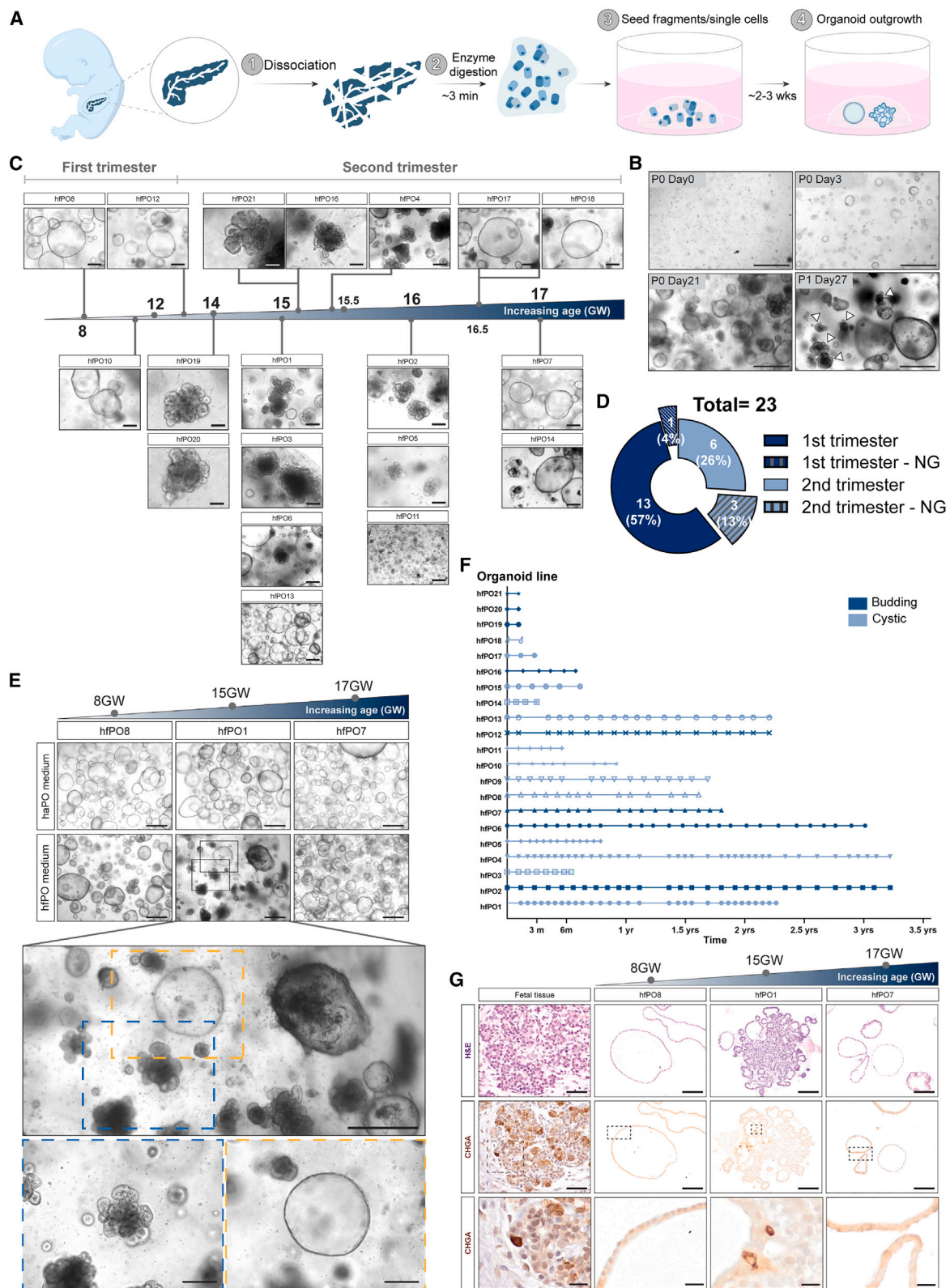
## INTRODUCTION

The mature pancreas performs two distinct functions: acinar cells of the exocrine pancreas secrete digestive enzymes, which are transported to the duodenum through ducts formed by ductal cells, while endocrine cells secrete their hormones into the circulation.<sup>1</sup> Murine *in vivo* model systems have provided most insights into pancreatic development, including the identification of a single multipotent progenitor for the three main cell lineages.<sup>2–6</sup> Culturing of such progenitors from both embryonic<sup>7,8</sup> and adult mice<sup>9,10</sup> has been attempted but has so far not allowed their long-term expansion. The study of human pancreas biology, prompted by human-mouse differences,<sup>11–13</sup> has historically been restricted largely to morphological approaches.<sup>11,14,15</sup> Recent transcriptome studies have delineated potential differentiation trajectories,<sup>16–19</sup> while differentiation protocols of human

pluripotent stem cells (hPSCs) have provided insights particularly toward generating  $\beta$  cells.<sup>20–25</sup> In these human studies, multipotent progenitor status is typically inferred indirectly based on murine marker genes.

Organoid technology allows modeling of organ development and maintenance in a dish.<sup>26,27</sup> Organoids can be grown either from induced PSCs (iPSCs) or from tissue-resident stem cells (TSCs). Research on the development, physiology, and pathology of the human pancreas would benefit from the availability of *in vitro* experimental platforms that faithfully replicate the cellular heterogeneity of the pancreas. Most state-of-the-art model systems focus on the generation of the insulin (INS)-producing  $\beta$  cell because of its involvement in diabetes. These model systems typically start from iPSCs<sup>20–25</sup> or employ transdifferentiation of other endocrine,<sup>3,28,29</sup> mesenchymal,<sup>30</sup> or endodermal cell lineages.<sup>31–34</sup> A recent study describes





(legend on next page)

steps toward the creation of whole pancreatic organoids from iPSCs. These organoids consist of progenitors as defined by marker analysis (but also contain mesodermal elements) and are capable of expanding over three passages.<sup>17</sup> While PSC-derived pancreatic progenitor spheroids can be passaged for longer time periods, they are restricted to the endocrine lineage as their main use has been in the generation of  $\beta$  cells.<sup>35–38</sup>

We have previously established organoids from adult mouse and human primary pancreas TSCs.<sup>39,40</sup> While these organoids can be cultured long-term, they remain fated toward the ductal lineage *in vitro*, and both acinar and endocrine cells are absent. This “*in vitro* unipotency” also holds true for the recently established murine islet organoids, which are restricted to the endocrine lineage.<sup>41</sup> Attempts to generate organoids from fetal human pancreatic tissue have had limited success as these have not been cultured long-term, lack acinar cells, and display limited capacity to generate endocrine cells.<sup>17,42,43</sup> Furthermore, the existence of a human tripotent stem/progenitor cell remains to be established.<sup>44–46</sup> Here, we aim to generate an *in vitro* model system from naturally specified fetal pancreas TSCs that mirrors the complexity of the epithelial pancreas.

## RESULTS

### Long-term culture of hfPOs

Human fetal pancreatic tissue from the first and second trimesters (obtained under informed consent) was processed and embedded in a basement membrane extract (BME) matrix (Figure 1A). Of note, the two latest lines were established in BME (Cultrex), but the others in Matrigel. We tested ~40 compound combinations and variations on the original medium for human adult pancreatic organoids (haPOs)<sup>39,40</sup> (Table S1). After 3 days, small cystic structures appeared under most medium conditions (Figure 1B). After 10–14 days, we observed the appearance of dark, budding grape-like structures in only one of the media, hereafter called human fetal pancreas organoid (hfPO) medium (see STAR Methods and Table S1 for its composition). To prevent the slower-growing budding organoids from being outcompeted by the fast-growing cystic organoids, we resorted to manual picking. Repeated handpicking yielded homogeneous budding organoid lines at later passages, while cystic organoids remained homogeneous with no *de novo* appearance of budding organoids. Cystic organoids grew to a size range of ~250–500  $\mu\text{m}$  and could be passaged 1:4–1:6 every 10–15 days. Budding organoids reached a size range of 150–350  $\mu\text{m}$  and could be passaged 1:3–1:5 every 20–30 days. Of note, budding organoids occasionally gave rise to cystic organoids upon passaging (which were removed by subsequent

picking). Organoids were karyotyped after 6 months in culture. One cystic line showed an abnormal karyotype and was excluded from further experiments. The same line also displayed a significantly faster growth rate compared with other lines.

A small biobank of 18 hfPO lines (Table S2) was established from 20 independent tissue samples spanning gestation weeks (GWs) 8–17 (Figures 1C, 1D, and S1A–S1C). Budding organoids only appeared in cultures derived from the 14–16 GWs samples (Figures 1E and S1A). Of note, the GW 14 line was only derived toward the end of the study and was not further characterized. hfPOs of both morphologies could be cultured long-term (>2 years) with no change in growth speed (Figures S1E and S1F), with the exception of one cystic line showing a decrease in growth speed 3 months before coming to a halt after 2.3 years in culture. The “oldest” budding line has been in continuous culture for ~3 years (Figure 1F; Table S2). hfPOs lines were tested for their ability to grow after being frozen for 2.5 years. Following initial recovery characterized by slightly lower growth speed (thawed organoids required an additional 5–7 days to reach their “passage ready” size), the organoids resumed their normal proliferation rate (Figure S1C). Organoids frozen as small fragments showed higher recovery rates compared with the same line frozen as single cells. Histological analysis of the organoid lines suggested that budding organoids more closely recapitulated fetal tissue architecture than cystic organoids did. Encouragingly, we observed the presence of rare chromogranin-A (CHGA, a marker of endocrine cells)-positive cells, exclusively in the budding organoids (Figures 1G and S1D).

### Budding organoids express acinar progenitor markers

After confirming widespread expression of the pancreatic marker gene PDX1 (Figure S2A) in all tested hfPO lines, we aimed to assess the difference between budding and cystic hfPOs. Budding and cystic hfPOs from the same line (hfPO1, hfPO2, hfPO5) and cultured in the same (hfPO expansion) medium, as well as hfPOs from purely cystic lines (hfPO7, hfPO8) were manually isolated and analyzed by bulk mRNA sequencing (mRNA-seq) (Figure 2A, S2B, and S2C). Transcriptome profiles demonstrated that cystic and budding hfPOs clustered separately (Figure 2B). Differential gene expression analysis showed that expression of acinar markers (carboxypeptidase A1 [CPA1], RBPJL, and PTF1A) was more prominent in budding hfPOs, whereas expression of ductal markers (keratin 7 [KRT7], mucin 1 [MUC1], and CEACAM6) was lower in comparison to cystic hfPOs (Figures 2C and 2D). We observed expression of endocrine markers (NEUROG3, CHGA, and CHGB) in budding hfPOs (Figure 2D). Notably, neither hfPOs derived from younger (8 GWs) nor older (17 GWs) fetal tissue samples expressed

### Figure 1. Establishment of hfPOs

- (A) Workflow of hfPO establishment.  
 (B) Representative images of hfPO1 outgrowth over time. White arrowheads indicate budding organoids.  
 (C) Representative bright-field images of established hfPO lines cultured in hfPO medium.  
 (D) Success rate of hfPO establishment from the first and second trimesters. NG, no growth.  
 (E) Representative images of hfPO lines from 8, 15, and 17 GW fetal pancreas tissue seeded in haPO and hfPO medium.  
 (F) Time in culture of hfPO lines. Darker blue lines: budding hfPO lines. Light blue lines: cystic hfPO lines. Each symbol represents a passage.  
 (G) Representative hematoxylin and eosin staining and immunohistochemical staining for CHGA of human fetal pancreas tissue (15 GW) and hfPO lines from 8, 15, and 17 GW. Scale bars, 500  $\mu\text{m}$  (B), (C), (E), and (G); scale bars, 500  $\mu\text{m}$  for all but hfPO19, 20, and 21, where it is 100  $\mu\text{m}$ . See also Figure S1 and Table S1.

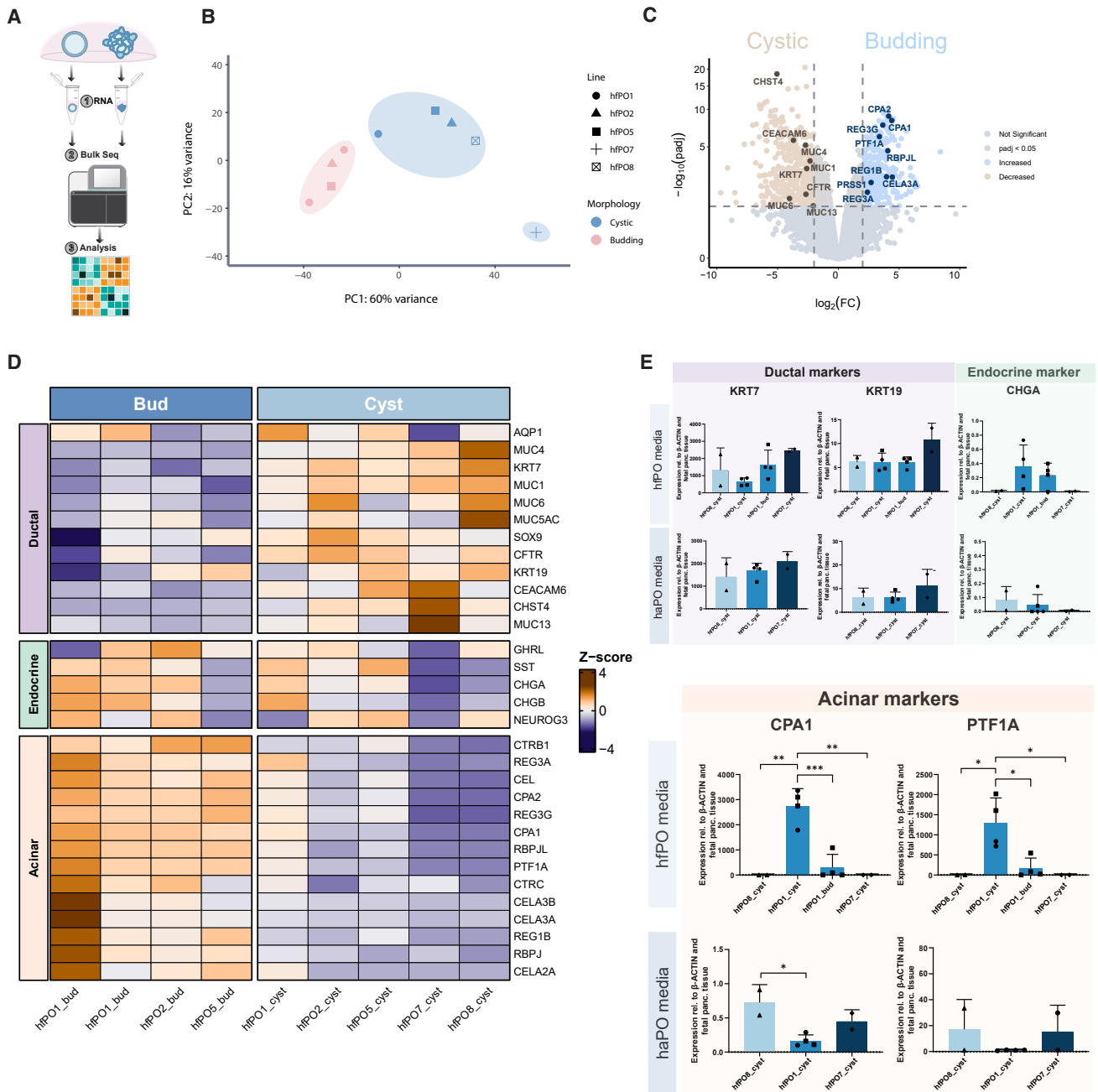


**Figure 2. Budding hfPOs are distinct from cystic hfPOs**

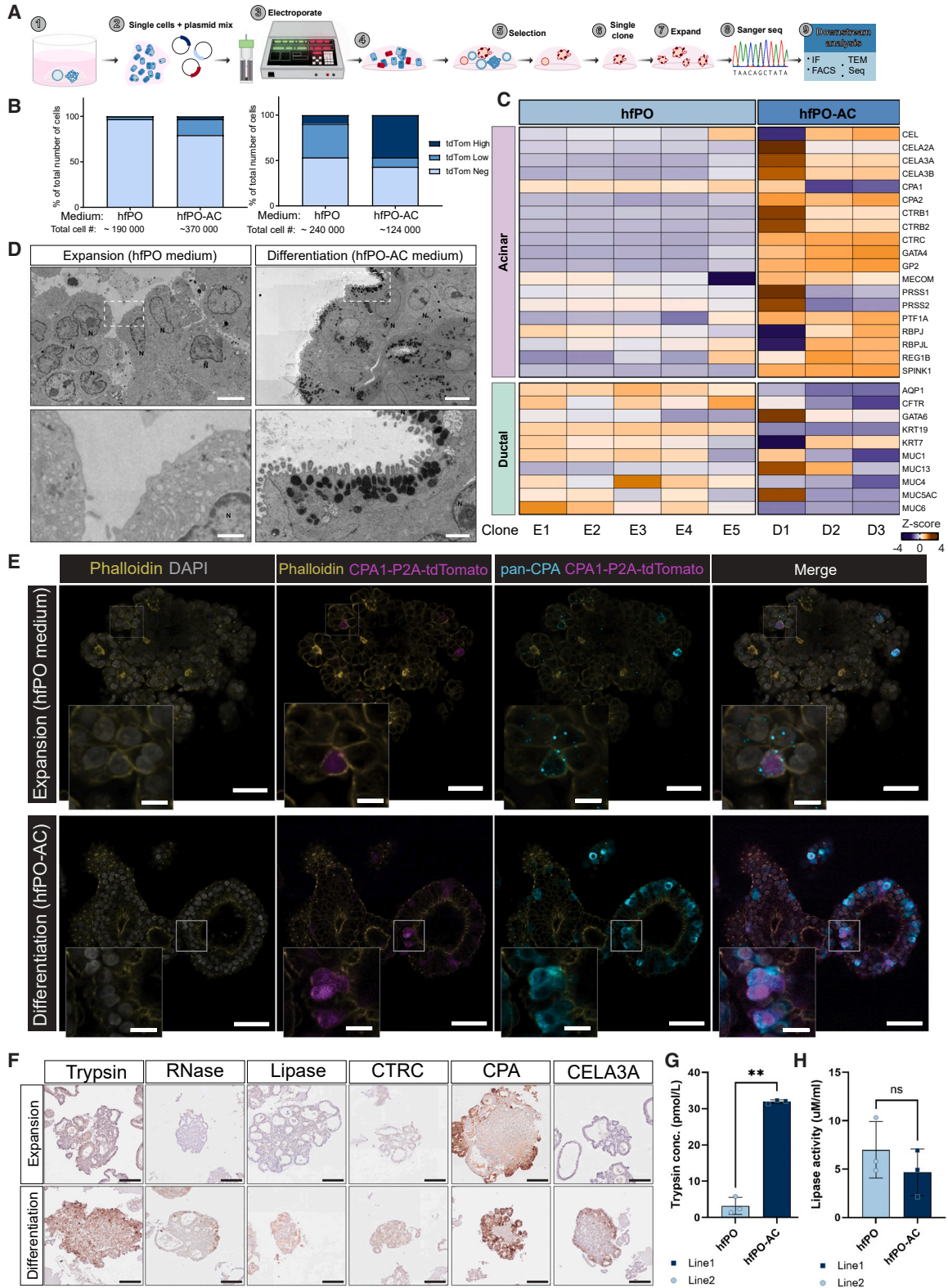
(A) Schematic of experimental approach.

(B) Principal-component analysis (PCA) plot of budding and cystic hfPOs.

(C) Transcriptional changes between budding and cystic hfPOs cultured in hfPO medium. Log<sub>2</sub> fold change on the x axis and the -log<sub>10</sub> adjusted *p* value on the y axis. *p* value of 0.05 and fold change of 2 are indicated by gray lines.

(D) Heatmap of differentially expressed genes (DEGs) of the acinar, ductal, and endocrine lineages between cystic and budding hfPOs cultured in hfPO medium.

(E) RT-qPCR analysis of KRT7, KRT19, CHGA, CPA1, and PTF1A in hfPOs derived from tissue samples of 8 GW cystic organoid (hfPO8), 15 GW budding, and cystic organoids (hfPO1 and hfPO4), minimum two wells from each line, technical triplicates. Each symbol is an individual well and 17 GW cystic organoids (hfPO7) cultured in hfPO medium. Each symbol represents an organoid line. Data for each line is from two different wells, and then technical triplicates. Data are represented as mean ± SD. \**p* < 0.05, \*\**p* < 0.01, \*\*\**p* < 0.001. For bulk-seq analysis (A–E), *n* = 3 (hfPO1, 2, and 5) for budding organoids and *n* = 5 for cystic organoids (hfPO1, 2, 5, 7, and 8). See also Figure S2.



(legend on next page)

acinar or endocrine progenitor genes. Also, hfPOs from 15 to 16 GWs samples cultured in the original haPO medium did not express acinar or endocrine progenitor genes (Figure 2E). Thus, haPO medium supported a ductal fate, whereas the hfPO medium allowed the expression of markers of all three pancreatic cell lineages, yet uniquely in 15–16 GWs-derived organoid lines. As organoid lines consisting of ductal cells have been established previously, we henceforth decided to focus on the budding lines from 15 to 16 GWs.

### hfPOs generate cells of the acinar lineage

Acinar cells have proven notoriously difficult to culture long-term. Following isolation, mature acinar cells are either short lived<sup>47</sup> or transdifferentiate into ductal cells.<sup>47–49</sup> To date, few human iPSC-based differentiation protocols exist for generating acinar cells *in vitro*,<sup>50</sup> and no protocol allows long-term co-existence of acinar, ductal, and endocrine cells. To our knowledge, no *in vitro* culture system exists that supports the *de novo* generation and subsequent differentiation of acinar cells from human TSCs.

Given the expression of acinar progenitor markers in hfPO cultures, we sought to promote further maturation into acinar cells able to produce digestive enzymes. To enable easy visualization and quantification of acinar cell formation without terminating the culture, we applied CRISPaint<sup>51,52</sup> to C-terminally tag the acinar genes CPA1 and PTF1A with the fluorescent protein tdTomato, preceded by a P2A self-cleaving peptide. This also allowed for subsequent isolation and analysis of cells expressing these acinar genes (Figures 3A and S3A–S3F). Following exposure of hfPOs to a growth factor-depleted differentiation medium (hfPO-AC) medium for 7 days, an increase of both gene expression levels as well as the number of CPA1<sup>+</sup> and PTF1A<sup>+</sup> cells was observed using fluorescence microscopy and fluorescence-activated cell sorting (FACS) analysis (Figures 3B, 3C, and S3G). This was further confirmed by bulk mRNA-seq (Figures S3C and S3G–S3I), which revealed upregulation of genes related to acinar cells (Figure S3I) as well as expression of digestive enzymes (e.g., CTB/C, CEL, and CEL2A/3A) (Figure 3C). More mature acinar cells are characterized by the presence of dark zymogen granules, in which digestive enzymes are stored pre-release.<sup>53,54</sup> To determine whether differentiation of hfPOs led to the formation of such granules, we performed transmission electron microscopy (TEM). This revealed the presence of secretory vesicles as a further sign of maturation (Figure 3D). Immunogold revealed that some of these vesicles were positive for

the digestive enzyme CPA (Figure S3J). Additionally, whole-mount immunofluorescence was used to visualize CPA1<sup>+</sup> and PTF1A<sup>+</sup> cells and confirm protein expression (Figures 3E and S3K). We observed some PTF1A-tdTomato<sup>+</sup> and CPA1-tdTomato<sup>+</sup> cells under hfPO expansion medium conditions (Figure S3K). This was not unexpected, as PTF1A is known to be expressed by some pancreas progenitor and acinar progenitor cells, yet at a lower level compared with more mature acinar cells.<sup>55–57</sup> Together, this confirmed differentiation along the acinar lineage. We observed increased expression of the digestive enzymes trypsin, RNase, lipase, chymotrypsin (CTRC), and chymotrypsin-like elastase 3A (CELA3A) at protein level (Figure 3F) as well as an increase of the numbers of cells expressing digestive enzymes (Figures S3L–S3N). Enzyme secretion for trypsin and lipase was assessed by ELISA and enzyme activity assay. We noted a significant increase in trypsin upon differentiation. While lipase was secreted under both expansion (hfPO medium) and differentiation (hfPO-AC) medium, the enzyme activity did not change significantly between the two conditions.

### hfPOs generate cells of the endocrine lineage

The presence of rare CHGA<sup>+</sup> cells in expansion medium suggested that the hfPOs also can generate endocrine cells. To investigate this further, we took inspiration from previously published hPSC  $\beta$  cell differentiation protocols<sup>20,21,58</sup> (hfPO-EC medium). To enable identification and isolation of endocrine cells following differentiation, we first generated endocrine reporter hfPO lines (Figures 4A and S4A). Following selection and expansion of clonal CHGA-hfPO reporter organoids, we observed rare dTomato<sup>+</sup> cells in expansion medium. This number increased ~5–10 $\times$  following 7–10 days in hfPO-EC medium (Figures 4B and S4B). By mRNA bulk-seq, hfPOs cultured in expansion vs. differentiation medium clustered separately (Figures 4C, S4C, and S4D), and genes involved in pancreatic endocrine function were upregulated in differentiation medium (Figure S4E). We observed increased expression of CHGA as well as appearance of mRNAs for the pancreatic hormones GCG, INS, somatostatin (SST), GHRL, and PPY (Figures 4D and 4E). Furthermore, TEM demonstrated the presence of vesicles characteristic of endocrine cells (Figures 4F and S5F). Immunofluorescence revealed the presence of poly- and mono-hormonal cells (Figure 4G). Of note, immature endocrine cells are known to be polyhormonal.<sup>59</sup> Expression of the endocrine-lineage master transcription factor NEUROG3<sup>60</sup> further supported ongoing neogenesis of early endocrine cells (Figures 4D, 4E, and S4). The potency of the

### Figure 3. hfPOs differentiation toward the acinar lineage

(A) Workflow to generate hfPO reporter lines.

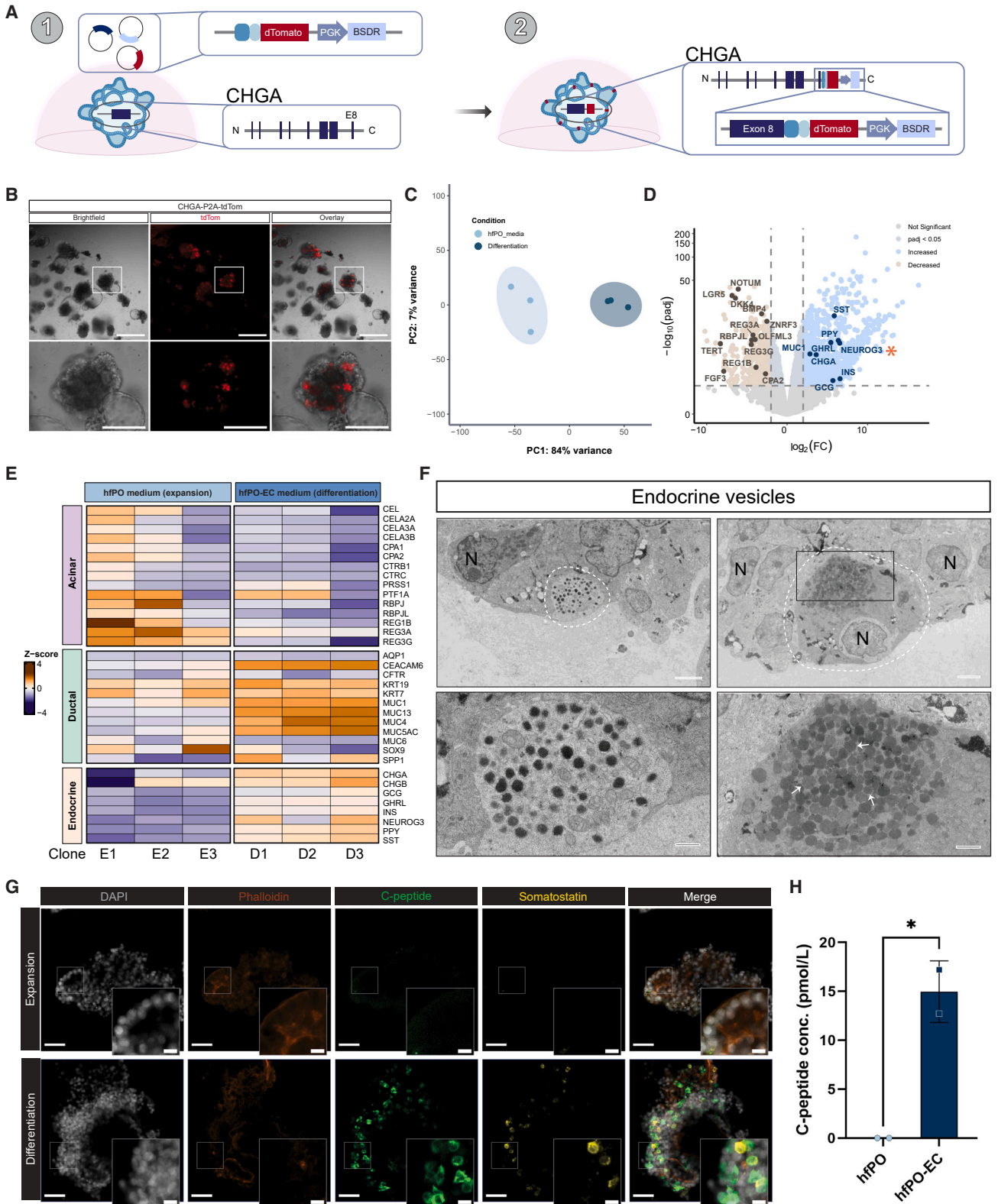
(B and C) Ridge plots showing the expression of CPA1 (B) and PTF1A (C) as measured by tdTomato fluorescence and quantification of negative (Neg), medium (Low), or high (High) expression of the reporter. PTF1A reporter generated in hfPO1 and hfPO2, experiment repeated twice, two clones from each line. CPA1 reporter generated in hfPO2, experiment repeated for 3 reporter clones, and for two clones, the experiment was performed twice.

(D) Heatmap of differentially expressed acinar and ductal genes in expansion ( $n = 5$  different PTF1A reporter lines cultured in hfPO expansion medium) or hfPO-AC differentiation ( $n = 3$  different clones from the PTF1A reporter hfPO1 line cultured in hfPO-AC medium). Of note, for the endocrine-related genes only CHGA and CHGB were detected, with an increased expression of CHGA upon differentiation. CHGB remained unchanged.

(E) TEM images of hfPOs cultured in hfPO and hfPO-AC medium (representative images from  $n = 4$ ).

(F) Immunofluorescence of CPA1 reporter organoids in hfPO and hfPO-AC medium (hfPO1 line, experiment repeated 3 times).

(G and H) Bar graph showing the trypsin concentration (G) lipase activity (H) in supernatants, measured by ELISA, from hfPOs cultured in expansion (hfPO) and differentiation (hfPO-AC) medium. Three biological replicates, technical duplicates. Data are represented as mean  $\pm$  SD. \*\* $p < 0.0035$ . Scale bars, 500 nm, top right; 100 nm, bottom right (D); 250 nm, top left; 125 nm, bottom left (D); and 50 and 12.5  $\mu$ m, inserts E100  $\mu$ m (F). See also Figure S3.



(legend on next page)

hfPOs to generate endocrine cells persisted in culture, as RT-qPCR showed that hfPOs could still generate INS-producing cells after 2 years *in vitro* expansion (Figure 6K). Accordingly, rare CHGA-P2A-tdTomato<sup>+</sup> cells remained present in expansion conditions during these 2 years. As organoids differentiate and mature, their proliferative capacity tends to decrease.<sup>61</sup> This held true also for hfPOs, as the number of proliferative MKI67<sup>+</sup> cells decreased upon culture in hfPO-AC and hfPO-EC medium (Figures S4G and S4H), whereas the number of CHGA<sup>+</sup> (endocrine marker) cells increased upon differentiation (Figures S4I–S4L). Finally, ELISA for c-peptide showed that hfPOs are able to produce and secrete c-peptide upon differentiation (Figure 4H). Together, this supported that hfPOs are able to generate more differentiated endocrine cells.

#### hfPO cells recapitulate key aspects of primary human fetal pancreas tissue

To determine if hfPOs recapitulate human fetal pancreas tissue, we performed vast transcriptome analysis of single cells by dA-tailing (VASA-seq), an single-cell RNA sequencing (scRNA-seq) technology that provides full transcriptome spliced and unspliced transcript reads.<sup>62</sup> As VASA-seq utilizes 384-well cell capture plates following FACS sorting, the total number of cells is lower compared with those commonly generated by 10x. However, the spliced/unspliced transcript information is crucial for unbiased analysis using trajectory inference algorithms such as Velocity<sup>62</sup> and scVelo.<sup>63</sup> We compared the transcriptome of our hfPOs grown in hfPO- or hfPO-EC medium to published human fetal pancreas tissue datasets<sup>16,18</sup> derived from comparable stages of development (Figures 5A and S5A). As hfPOs contain only epithelial cells (mesenchymal cells are lost during the initial passages), we extracted the epithelial cells from the published datasets by removing mesenchymal, endothelial, and immune cells.<sup>16,18</sup>

Following quality control (Figures S5A and S5B), the three datasets were merged into a final dataset containing 11,755 cells of which hfPOs represented almost 20% (Figure 5A). Dimensional reduction demonstrated high overlap between hfPOs and fetal tissue cells. The Xu dataset<sup>18</sup> contains samples covering a broad range of GWs, and, as expected, the hfPOs showed best overlap with time points closest to the fetal tissue sample from which the organoids were derived (Figures 5B and S5C–S5E). Consequently, we selected those time points (14 and 16 GWs) for in-depth analysis. Unsupervised hierarchical clustering identified four main clusters. Three of these clusters corresponded to the

three main pancreatic cell lineages, whereas the fourth cluster expressed progenitor markers such as SOX9 and PROM1 (Figures 5C and 5D). Cells from each dataset contributed to all clusters, with the hfPO cells showing a relatively higher contribution to the progenitor cluster (Figure 5E) (unsurprisingly so, since continuous TSC-derived organoid culturing specifically drives stem/progenitor cells).

Marker genes for known murine pancreas multipotent progenitor cells (HNF1 $\beta$ , GP2, GATA4/6, PDX1, SOX9) were expressed by hfPO cells in the stem/progenitor cluster as well as by stem/progenitor cells from the two human fetal pancreas datasets<sup>16,18</sup> (Figures 5D and S5F). In accordance with previous studies,<sup>14,55–57,64</sup> expression of PTF1A and CPA1 was lower in the progenitor cell cluster with higher levels observed in the acinar cell, coinciding with expression of digestive enzymes (PRSS1, CEL, CELA3A). This supported the presence of acinar progenitors (Figures 5D and S5E). GP2, a reported marker for murine multipotent progenitor cells and, at later stages, for acinar cells<sup>65,66</sup> displayed a similar expression pattern (Figure S5G). The transcription factors GATA4/6 also exhibited the expected expression pattern: Initially being co-expressed at low levels, GATA4 increased and became restricted to the tip (acinar) compartment, whereas GATA6 localized to the trunk (ductal and endocrine) compartment<sup>67</sup> (Figures 5D and S5G). Importantly, comparison of the cell lineage composition of the pancreatic epithelium from adult<sup>68,69</sup> and fetal<sup>19,70</sup> pancreas tissue to that of the hfPOs (cultured in expansion hfPO medium) showed that the proportion of the different cell lineages of the hfPOs more closely resembled fetal pancreas tissue (Figure 5F). Genes related to the acinar lineage identity and function (such as PRSS1, CEL, and CTSC) were among the most differentially expressed genes between adult and first-trimester fetal tissue (Table S3). These genes were also among the most differentially expressed genes when comparing adult tissue to hfPOs (Table S4).

To compare our hfPOs to fetal and adult pancreas tissue, we performed immunohistochemical stainings (Figure 6A). This revealed both structural and marker gene expression differences. Overall, hfPOs were more similar to fetal tissue, especially in their higher KRT19 expression as well as the scattered expression of CHGA, while, in comparison, CHGA was restricted to the islets in the adult tissue. Fetal tissue expressed almost no lipase and RNase. However, upon differentiation, hfPOs upregulated the expression of lipase and RNase, making them more similar to adult tissue (although absolute levels of expression remained

#### Figure 4. hfPOs can be differentiated toward the endocrine lineage

(A) Schematic of hfPO CHGA reporter generation.

(B) Representative bright-field and fluorescent images of a CHGA-P2A-tdTom hfPO1 reporter line.

(C) PCA plot of hfPO lines cultured in hfPO- and hfPO-EC medium.

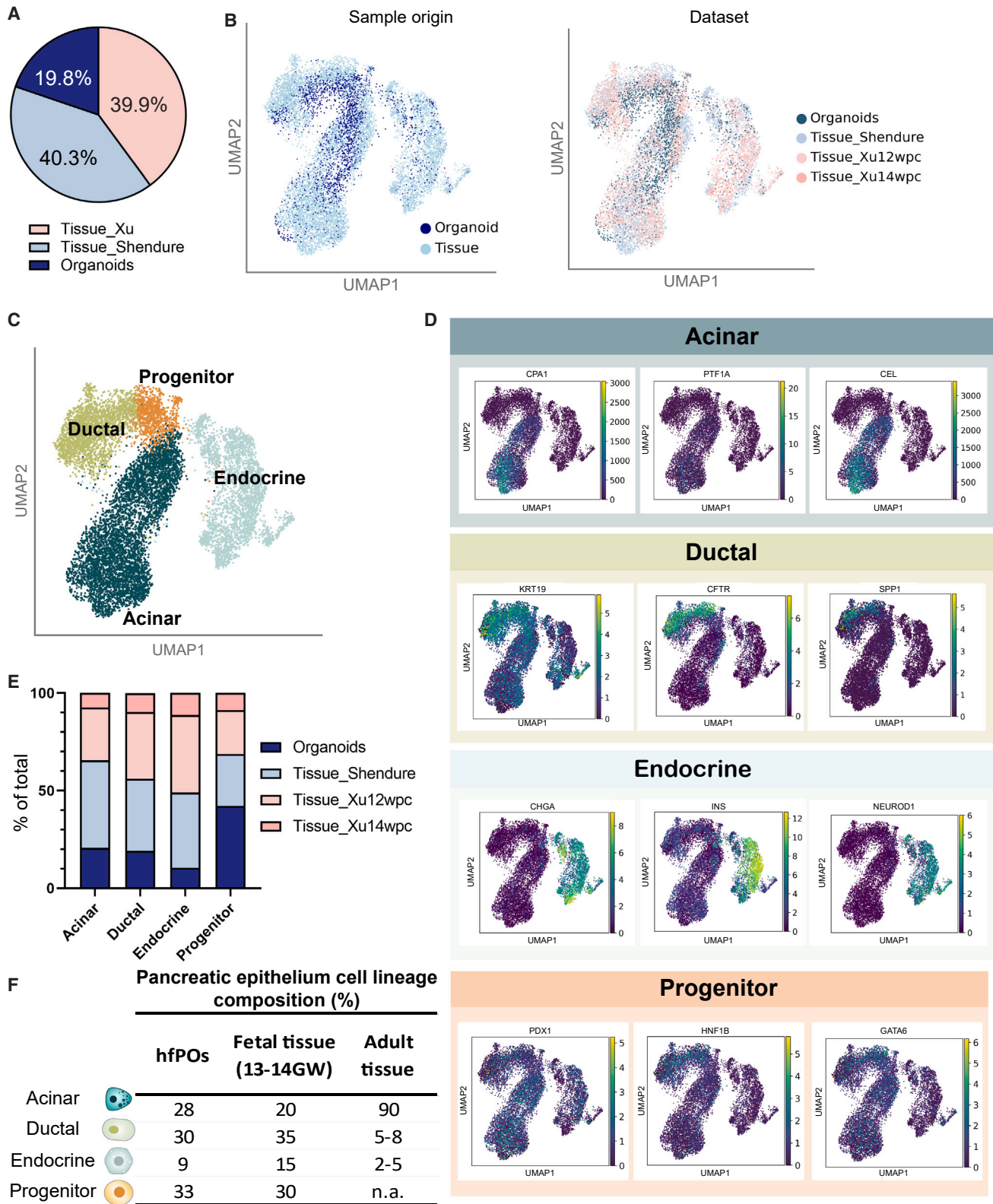
(D) Transcriptional changes between hfPOs cultured in hfPO- and hfPO-EC medium. Log<sub>2</sub> fold change on the x axis and the  $-\log_{10}$  adjusted *p* value on the y axis. *p* value of 0.05 and a fold change of 2 are indicated by gray lines.

(E) Heatmap of DEGs of the acinar, ductal, and endocrine lineages in hfPO and hfPO-EC medium.

(F) Representative TEM images of hfPO1 cultured in hfPO-EC medium (repeated twice and in 3 different lines). White arrows point to vesicles.

(G) Confocal images of hfPO1 organoids cultured in hfPO- and hfPO-EC medium, stained for DAPI, phalloidin, and the endocrine hormones insulin (c-peptide) and somatostatin (representative images from *n* = 3, for the CHGA reporter, 3 different clones per line).

(H) Concentration of c-peptide in organoid supernatant. Data are represented as mean  $\pm$  SD. \**p* < 0.0045. Scale bars, 500 and 200  $\mu$ m (B), 200 nm (top), and 50 nm (bottom) for the left panels; 2550 nm (top) and 100 nm (bottom) for the right panels; N, nucleus (F), 50  $\mu$ m (G). For the bulk-seq analysis (C–E), 3 different hfPO1 CHGA reporter clones were used. The endocrine-lineage master transcription factor NEUROG3 is indicated with an orange asterisk. See also Figure S4.



(legend on next page)

lower). Immunofluorescence of fetal tissue and hfPOs showed the presence of both acinar and ductal cells, with the appearance of acinar cells predominantly appearing in the budding structures (Figure 6B). To further assess the similarity of the different cell lineages generated in culture to those of the fetal and adult pancreas on the transcriptome level, we included a published dataset of healthy human adult pancreas.<sup>71</sup> Again, we excluded non-epithelial pancreatic cells (mesenchymal, neural, and blood cells) from the tissue datasets prior to the analysis. A panel of markers representing the different pancreatic cell lineages was compiled based on previously published studies<sup>16,17,72–74</sup> (Figures 6C and S6). Following exposure to hfPO-AC differentiation medium, hfPOs upregulated processes related to pancreatic secretion and protein digestion and absorption (Figure S6A). Comparison of acinar cells from hfPOs, fetal (first and second trimesters), and adult pancreas tissue revealed that overall, the hfPO-generated acinar cells closely resembled fetal pancreas tissue from the first trimester, both in terms of the genes being expressed as well as their expression levels. Fetal tissue from later stages of the second trimester more closely resembled adult human tissue (Figure 6C). Expression of the human cationic trypsinogen (PRSS1) was highest in acinar cells from the late second trimester and adult tissue (Figure S6B). However, it was also more highly expressed in hfPOs compared with first-trimester and early second-trimester fetal tissue, as seen at transcript- and protein level comparing fetal tissue and hfPOs (Figure 6C). In addition, hfPOs were able to produce other digestive enzymes such as serine protease chymotrypsinogen B1 (CTRB1), CTRB1, and the CELA3A (Figures 6A and S6B). XBP1 showed a similar expression level pattern, indicating that while hfPO-derived acinar cells overall mimic first-trimester fetal tissue, some cells representing later stages of development can be present. A previous study has shown that adult acinar cells commonly express either PRSS1 or REG3A and that double expressers are rare.<sup>75</sup> To investigate whether this heterogeneity was already present during early development of the human pancreas, we further subclustered hfPO-derived acinar cells. This did not result in distinct clusters based on PRSS1 or REG3A expression. Instead, the majority of the acinar cells co-expressed PRSS1 and REG3A, with a smaller fraction expressing only PRSS1. Although not mutually exclusive, higher expression levels of a certain group of digestive enzymes correlated with a lower expression of other enzymes. For example, cells expressing high levels of elastases such as CELA3A/B expressed lower levels of trypsinogens such as PRSS1/2 and vice versa (Figure S6C). Together, these results indicated that hfPO-generated acinar cells recapitulate the endogenous first-trimester acinar cells yet were able to produce different digestive enzymes similar to those of later-stage fetal tissue.

hfPO-derived ductal cells closely resembled first-trimester-tissue-derived ductal cells (Figure 6D) and produced MUC1. Known for being one of the most predominantly expressed mucins of normal pancreatic ducts, MUC1 serves as a protective barrier in order to maintain the structural integrity of the ductal epithelial lining.<sup>76,77</sup> As in fetal tissue, MUC1 located on the apical membrane in the hfPOs (Figures S6B and S6D). Cystic organoids consisted entirely of ductal cells, as seen by the expression of the ductal marker KRT19 and the absence of the acinar marker CPA1. In the rare cases where acinar cells were present in cystic organoids, they were positioned in “folded” areas (Figure S6D).

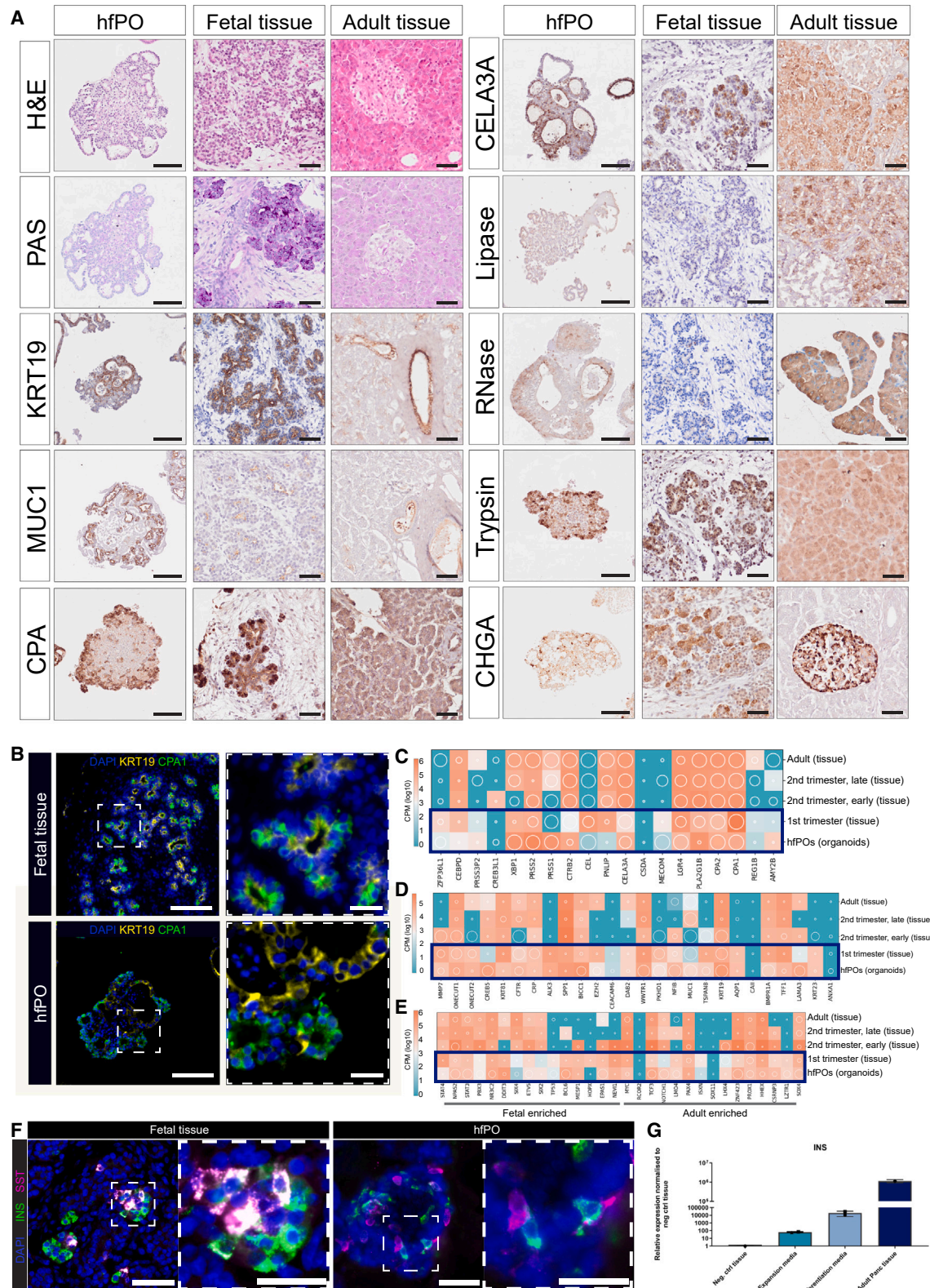
Following the trend of the acinar and ductal lineages, hfPO endocrine cells mimicked those of the first-trimester fetal pancreas tissue (Figures S6E–S6G). This specifically held also for hfPO-derived  $\beta$  cells, when assessed for markers related to adult and fetal beta cells (Figure 6I) as well as for key genes necessary for  $\beta$  cell function (Figures S6F and S6G). The ability of hfPO-derived  $\beta$  cells to produce INS was further confirmed at transcriptome and protein level (Figures 6F and 6G). Unsurprisingly, the expression level of INS was higher in adult tissue compared with that in fetal tissue and hfPOs (Figure 6G). Yet, the levels of endocrine progenitor markers NEUROG3 and FEV were higher in the organoids, indicating active generation of new endocrine cells. Overall, these data support the notion that hfPOs phenocopy the fetal state in terms of transcriptome profiles and digestive enzyme, mucous, and hormone production.

### LGR5 marks human tripotent stem cells

The ability of hfPOs to be cultured long-term, combined with their capacity to be fated toward ductal, acinar, and endocrine lineages, led us to search for a tripotent progenitor cell. We generated clonal organoids from single cells. These clonal organoids were expanded and exposed to either hfPO expansion medium (supporting acinar and ductal progenitors) or hfPO-EC medium (promoting a more mature endocrine fate) for 10 days before being subjected to scRNA-seq (Figure 7A). Post-quality control, the VASA-seq dataset, comprising reads from two individual clones, contained 2,458 cells, which separated into five main clusters representing progenitor, acinar progenitor, acinar, ductal, and endocrine cells (Figures 7B and S7B–S7E). Subclustering of the endocrine cluster allowed discrimination of endocrine progenitor genes (e.g., NEUROG3, NEUROD1, and FEV) and the different endocrine subtypes. In addition to  $\beta$  cells, we also observed, e.g.,  $\delta$  and  $\epsilon$  cells and their respective transcription factors (MAFA, HHEX, and PAX6, respectively) (Figure S7F). The presence of NEUROG3<sup>+</sup> cells agreed with the results of the previous bulk RNA-seq results and further supported the notion that the endocrine cells are generated *de novo* via

### Figure 5. hfPOs recapitulate human fetal tissue at single-cell transcriptome level

- Relative contribution of each individual scRNA-seq dataset to the final dataset.
- UMAP of the merged scRNA-seq dataset showing sample origin (tissue or organoids) (left) and different datasets (right).
- UMAP visualization of cell clusters (acinar, ductal, endocrine, and progenitor).
- Feature plots showing the expression of marker genes related to the clusters.
- Relative contribution of each dataset to each cluster.
- Percentage (%) of the different pancreatic cell lineages in hfPOs, fetal (13–15 GW), and adult tissue. See also Figure S5.



(legend on next page)

neogenesis rather than mitosis of pre-existing endocrine-fated cells. Analysis of the scRNA-seq endocrine cell clusters showed that ~50% of the cells within the cluster were endocrine progenitors. Thus, endocrine progenitors as well as more differentiated single hormone-producing cells co-existed upon exposure of hfPOs to differentiation medium (Figure S7G). This was further supported at protein level by the presence of polyhormonal (SST and c-peptide double-positive endocrine cells) as well as single hormonal cells (Figure 4H). Polyhormonal endocrine cells are known as transient, immature endocrine cells present during development.<sup>59,78</sup>

We then sought to reveal the identity of the tripotent stem cell. As dimensional reduction and its uniform manifold approximation and projection (UMAP) representation do not provide directionality with regards to lineage differentiation, we exploited the fact that VASA-seq provides spliced and unspliced transcript reads (Figure S7G). This allowed unbiased scVelo pseudotime analysis. While predicting that the “early time point” corresponded to the progenitor cluster and that later time points corresponded to the clusters representing the different cell lineages, pseudotime analysis gave no information regarding progenitor heterogeneity or potential hierarchy (Figure S7H). To further investigate progenitor trajectories heterogeneity, we utilized the VASA-seq data for analysis by RNA velocity.<sup>63,79</sup> Trajectory inference analysis generated arrows originating from the progenitor cluster and pointing toward each of the three main lineage clusters (Figure 7B), suggesting a differentiation route originating from the top part of the progenitor cluster. Further subclustering of the progenitor cluster revealed that cells belonging to the top part of the cluster expressed high levels of two generic epithelial stem cell markers, leucine-rich repeat-containing G-protein coupled receptor 5 (LGR5) and TNF receptor superfamily member 19 (TROY) (Figure 7C), first discovered in intestinal stem cells.<sup>80,81</sup> Of note, we have shown previously that LGR5<sup>+</sup> cells appear following injury of the adult pancreas.<sup>40</sup> These markers, especially LGR5, appeared more restricted to the initial progenitor state (based on velocity analysis and gene expression levels) than the “classical” fetal pancreas progenitor markers (PROM1,<sup>82</sup> GP2,<sup>65,83,84</sup> HNF1 $\beta$ ,<sup>85</sup> PDX1,<sup>5</sup> SOX9<sup>86,87</sup>), which were expressed much more broadly and typically increased going from LGR5<sup>+</sup> to LGR5<sup>-</sup> compartments (Figures S8E and S8F). Although PTF1A and GP2 are known multipotency markers in mice, they were not among the top 50 most highly expressed in the LGR5<sup>+</sup> cells, thus indicating that species-specific differences might exist.

Before assessing the potency of LGR5<sup>+</sup> and TROY<sup>+</sup> cells *in vitro*, we investigated their presence in human fetal pancreas tissue using scRNA-seq analysis. LGR5<sup>+</sup> cells were present within the scRNA-seq progenitor cluster, in a pattern that again suggested that LGR5<sup>+</sup> cells sit at the root of the stem cell hierarchy (Figure S7I). During pancreatic organogenesis, multipotent progenitor/stem cells are expected to be most abundant at the early stages when organ growth is most rapid. Indeed, LGR5 expression followed this temporal expression (Figure 7D). Consistent with previous studies, LGR5 and TROY were not expressed in healthy adult tissue. *In situ* hybridization by RNAScope visualized LGR5<sup>+</sup> and TROY<sup>+</sup> cells in fetal tissue (Figure 7E). The specificity of the LGR5 RNAScope probe was confirmed on human colon tissue (Figure S7J). Transcriptome comparison of LGR5<sup>+</sup> and LGR5<sup>-</sup> cells showed that SMOC2, TROY, and ZNRF3 were among the most upregulated genes in the LGR5<sup>+</sup> population (Table S5). Additionally, LRIG1<sup>88</sup> and RNF43 were also expressed (although not among the top 50 most differentially expressed genes). These genes are key determinants of LGR5<sup>+</sup> stem cells in the adult intestine.<sup>81,89,90</sup> TROY and LRIG1 also mark multipotent stem cells of the adult stomach<sup>91</sup> and epidermis,<sup>88</sup> respectively.

Since LGR5 surface staining is not possible due to vanishingly low surface expression levels (in contrast to TROY), we generated reporter LGR5-P2A-tdTomato reporter hfPO lines (Figure 7F) to be able to assess lineage potential following outgrowth of FACS-sorted individually seeded cells. The LGR5 reporter organoid lines were maintained and passaged similarly to reporter-negative lines, and LGR5<sup>+</sup> (tdTomato<sup>+</sup>) cells could be observed in the subsequent passages, showing that the LGR5<sup>+</sup> cells could be expanded long-term (current passage number post clonality and genotyping is 11). To assess lineage potential, we first seeded single LGR5-P2A-tdTomato<sup>+</sup> and FACS-sorted TROY<sup>+</sup> cells to assess their organoid-forming capacity, used as a proxy for stemness (Figure 7G, outgrowth assessed at step 3). LGR5<sup>+</sup> cells showed a significantly higher organoid-forming capacity compared with TROY<sup>+</sup> cells (21% compared with 4.3%, respectively) as well as to LGR5<sup>-</sup> and TROY<sup>-</sup> cells (2.2% and 1%, respectively) (Figures 7H, S7K, and S7L). Notably, while LGR5<sup>-</sup> and TROY<sup>-</sup> cells did form some organoids post-seeding, these typically did not continue to proliferate or form new organoids after the first passage. By contrast, the majority (~95%) of the LGR5<sup>+</sup> cells and (~80%) TROY<sup>+</sup> continued to proliferate and form new organoids post passaging.

### Figure 6. hfPOs recapitulate human fetal pancreatic tissue

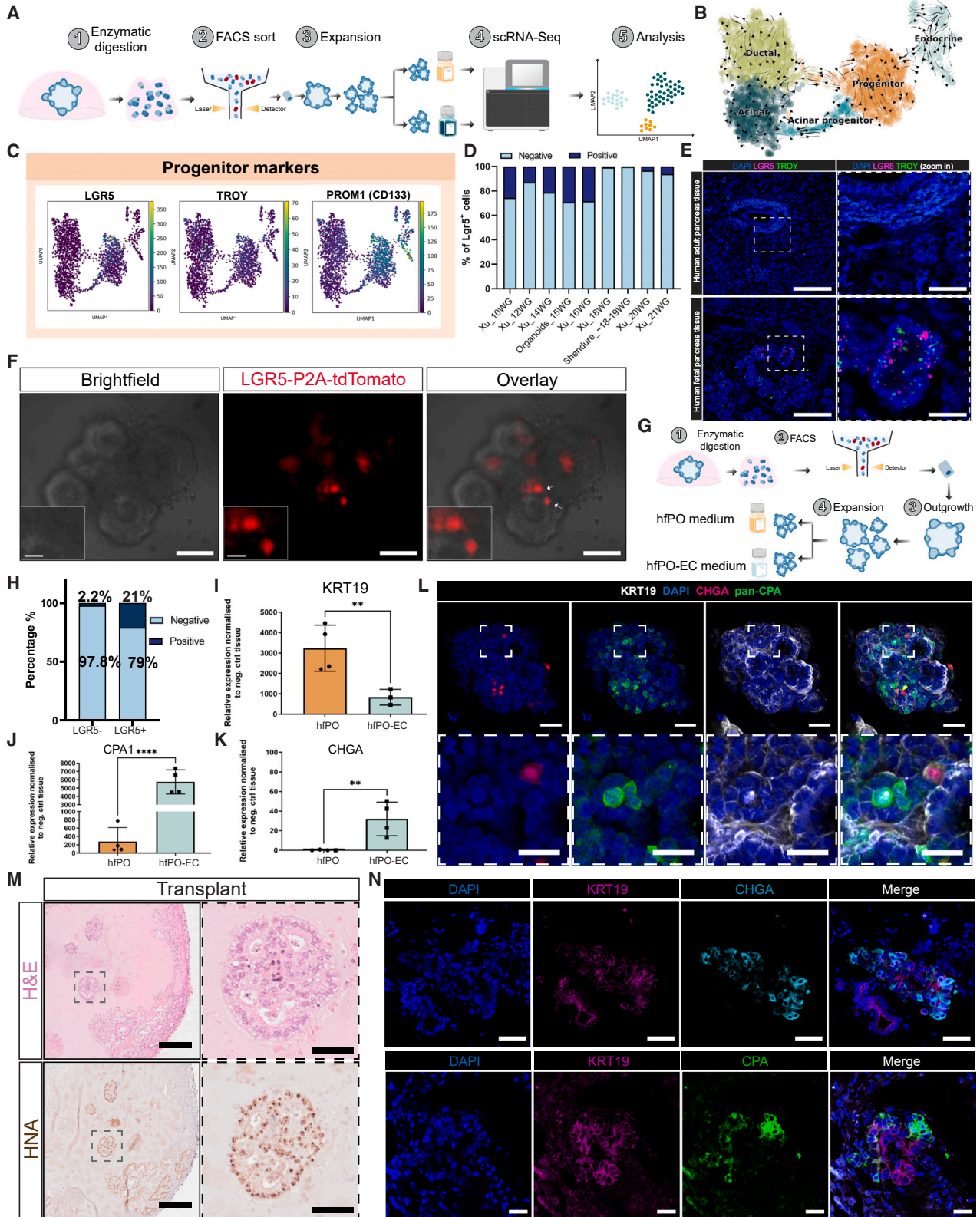
(A) Immunohistochemical stains comparing adult and fetal pancreatic tissue to hfPOs.

(B) Representative confocal images of human fetal pancreatic tissue and hfPOs stained for DAPI, keratin 19 (KRT19), and carboxypeptidase A (CPA). Scale bars, 100 and 20  $\mu$ m for zoom in. All IHC stainings, but MUC1, were performed on fetal pancreas tissue of 15 GW.

(C–E) The MUC1 staining was performed on fetal tissue from 16 GW. Expression profiles for key marker genes for the acinar (C), ductal (D), and endocrine beta cells (E). Shading displays mean expression (counts per million [CPM], log scaled), and diameter denotes fractional expression. Shading displays mean expression (CPM, log scaled), and diameter denotes fractional expression.

(F) Representative confocal images of human fetal pancreatic tissue and hfPOs stained for DAPI, c-peptide, and somatostatin (SST). Scale bars, fetal tissue 50 and 25  $\mu$ m for zoom in. hfPO 25 and 12.5  $\mu$ m for zoom in.

(G) RT-qPCR analysis of insulin (INS) of hfPOs in expansion (hfPO) and differentiation (hfPO-EC) medium. Two different hfPO lines were used. For the negative control (tongue), adult pancreas tissue commercially available pooled RNA from 5 different donors was used. Data are represented as mean  $\pm$  SD (for the negative control and adult pancreas tissue, technical replicates). Scale bars, hfPOs, 100  $\mu$ m, fetal and adult tissue, 50  $\mu$ m. See also Figure S6.



(legend on next page)

Following organoid formation, single-cell-derived LGR5 clonal organoids were expanded and exposed to either hfPO expansion medium (supporting acinar and ductal progenitors) or the hfPO-EC medium to promote endocrine/acinar differentiation for 10 days (Figure 7G). RT-qPCR showed that hfPO-EC medium increased the endocrine and acinar markers CHGA and CPA1, while simultaneously decreasing expression of the ductal marker KRT19. In hfPO medium, markers of all three lineages were expressed, although CHGA levels were very low, consistent with the rare occurrence of CHGA<sup>+</sup> cells under expansion conditions (Figures 7I–7K; Table S6). We confirmed these observations by whole-mount immunofluorescence confocal imaging of clonal CHGA reporter hfPO lines stained for KRT19 and pan-CPA (Figures 7L and S7M).

To assess the ability of hfPOs to also give rise to the three main pancreatic cell lineages *in vivo*, we transplanted hfPOs grown in expansion medium for 2 weeks post-split into the fat pad of NSG mice. We transplanted three independent organoid lines and observed an overall engraftment rate of 75% 8 days post transplantation (9/12 mice), and the presence of human cells was validated by immunohistochemistry (IHC) staining of human nuclear antigen (Figure 7N). Immunofluorescence stainings for ductal (KRT19), acinar (CPA), and endocrine (CHGA) markers confirmed the presence of the three main cell lineages (Figure 7N). Taken together, single LGR5<sup>+</sup> stem cells are capable of giving rise to hfPOs containing all three pancreatic cell lineages.

To further characterize the hfPOs derived from LGR5 reporter-positive cells, we compared them to hfPOs derived from the bulk human fetal pancreatic tissue in terms of yield (Figure S8A), post-split morphology (Figure S8B), and plating efficiency (Figure S8C). Overall, we did not detect any significant difference between LGR5-derived hfPOs and hfPOs derived from fetal tissue. Also, upon differentiation, LGR5-derived hfPOs (just like the hfPOs from fetal pancreas tissue) showed an increase in the expression of endocrine and acinar marker genes, also at protein level (Figure S8D).

To test the outgrowth efficiency of LGR5<sup>+</sup> cells directly from primary fetal tissue, we sorted LRIG1<sup>+</sup> and TROY<sup>+</sup> cells from 14 to 15 GWs primary fetal pancreatic tissue. The outgrowth efficiency of both LRIG1<sup>+</sup> and TROY<sup>+</sup> cells was higher compared with that of LRIG1<sup>-</sup> (Figure S8G) and TROY<sup>-</sup> (Figure S8H) cells (all cells were EPCAM<sup>+</sup>). Of note, the expression pattern of LRIG1 was broader compared with LGR5, while the outgrowth efficiency of LRIG1<sup>+</sup> cells from primary tissue was not higher than the outgrowth efficiency of LGR5<sup>+</sup> cells sorted from organoids at the 15 GWs time point (Figure S8I).

## DISCUSSION

Here, we describe highly stable organoid lines, uniquely derived from 15 to 16 GWs human fetal pancreas. Such organoid lines can be grown from single LGR5<sup>+</sup> tripotent progenitors, which maintain their capacity to generate acinar, ductal, and endocrine cells (Figure 7). Whereas mouse multipotent progenitors exist until the third quarter of the pregnancy, human multipotent progenitors disappear before midterm.<sup>1,14,92</sup> Histological studies and inference from the mouse developmental timeline have estimated that human tripotent progenitors exist up until ~14 GWs<sup>1,14,92</sup>; however, our findings would argue that they may persist until 15–16 GWs. The time window from which we derive hfPOs containing all main cell lineages likely reflects the moment of maximal presence of tripotent progenitors. Of note, we and others have noted that TSC-derived organoids representing several other organs tend to stay locked in the regional fate and developmental stage of the tissue from which they derive.<sup>93–99</sup> In line with these findings, hfPOs recapitulate the natural epithelial complexity of the human fetal pancreas. *In vivo*, lobule formation is initiated at ~14 weeks, after which acinar cells with zymogen granules become apparent. Prior to the 12–14 weeks time point, the pancreas consists almost exclusively of undifferentiated cells organized in tubules.<sup>100</sup> Consistent with this developmental timeline, we observe expression of multiple digestive enzymes produced by acinar

### Figure 7. LGR5 marks tripotent human pancreatic progenitors

- (A) Schematic image of generating single-cell-derived hfPO scRNA-seq data.  
(B) RNA velocity estimates (arrows) plotted on a UMAP with clusters. The transcription rate (velocity) is represented by the length of the arrows. The direction of the arrows points toward the velocity future state of the cell based on velocity calculations, taking into account all other cells.  
(C) UMAPs showing the expression of LGR5 and TROY as well as the classical progenitor marker CD133.  
(D) Percentage of Lgr5<sup>-</sup> and Lgr5<sup>+</sup> cells in the different datasets of different developmental stages.  
(E) Confocal images of adult and human fetal tissue (15.5 GW) stained for DAPI and RNAScope probes against LGR5 and TROY (representative images from  $n = 3$  different adult tissues and  $n = 2$  different fetal tissues of 15.5 and 15.8 GWs).  
(F) Representative bright-field and fluorescent images of an LGR5-P2A-tdTom reporter line (representative image from  $n = 3$  clonal lines).  
(G) Workflow to address tripotency. Following FACS sorting, single cells are cultured in individual drops of extracellular matrix to generate single-cell-derived clonal organoid lines. The clonal lines are expanded before being exposed to expansion (hfPO medium), differentiation (hfPO-EC medium), or adult (haPO medium) pancreatic organoid medium.  
(H) Bar graphs showing organoid-forming efficiency of FACS-sorted LGR5<sup>-</sup> and LGR5<sup>+</sup> single cells.  
(I–K) RT-qPCR analysis of CPA1, KRT19, and CHGA in FACS-sorted Lgr5 single-cell-derived clones cultured in hfPO- or hfPO-EC medium.  $n = 3$  or 4. Data are represented as mean  $\pm$  SD. \*\* $p < 0.0085$ , \*\*\*\* $p < 0.0001$ . Negative control tissue (tongue) from commercially available pooled RNA from 5 different donors was used.  
(L) Representative confocal images of a single-cell-derived hfPO whole mount stained for DAPI, KRT19, pan-CPA, and CHGA (experiment repeated 3 times).  
(M) Representative immunohistochemical images of H&E and human nuclear antigen on transplantation grafts in the mammary fatpad 8 days post transplantation.  
(N) Immunofluorescent stainings against ductal (KRT19), acinar (CPA), and endocrine (CHGA) markers of organoids present within the graft. Scale bars, 50  $\mu$ m and zoom in 25 (J), 50 (M), and 25  $\mu$ m (N).  
See also Figures S7 and S8.

cells, including trypsinogen (PRSS1 and PRSS2), proteases (CTRB1, CTRB2, and CTRC), and elastases (CELA2A and CELA3A/B).

The identification of LGR5<sup>+</sup> cells in primary fetal pancreas tissue as well as *in vitro* and their consistent assignment to the earliest progenitor cluster in both cases implies a role as the most primitive tripotent fetal pancreas progenitors. These cells precede the cellular states that are marked by commonly used markers such as PTF1A, PDX1, SOX9, HNF1 $\beta$ , MNX1, or by high expression of GATA4/6 and GP2. Most importantly, single LGR5<sup>+</sup> progenitor cells were able to generate organoids containing the three different cell lineages (acinar, ductal, and endocrine cells, providing evidence of their tripotency). Of note, LGR5<sup>80,101</sup> and TROY<sup>91,102</sup> are well-established, exquisite markers of the human small intestine, which generates all cell lineages of the gut epithelium, including the various enteroendocrine lineages.<sup>91,103,104</sup>

We anticipate that the long-term *in vitro* expansion capacity of these tripotent pancreas progenitors under defined conditions and the ease of their genetic modification will complement existing experimental platforms to study human pancreas development, physiology, and disease. Finally, this pancreas organoid platform may inspire regenerative efforts to restore pancreatic dysfunction of any of the three cellular compartments, either by cellular therapy or by targeted treatment with defined growth factor combinations. Such efforts will involve further improvements of maturation protocols.

### Limitations of the study

The hfPOs provide a platform to study the human fetal pancreas in health and disease and thus require human fetal tissue. Legal and ethical guardrails around human fetal tissue experimentation differ between geographies. We show that LGR5<sup>+</sup> cells are human tripotent pancreatic progenitors, yet their exact relation to other progenitor populations as well as the extent of plasticity of such populations deserves further investigation. Improvements of maturation protocols will be essential for the generation of exocrine/acinar and endocrine cells to match those of human adult tissue.

### RESOURCE AVAILABILITY

#### Lead contact

Further information and requests for resources and reagents should be directed to the lead contact, Hans Clevers ([h.clevers@hubrecht.eu](mailto:h.clevers@hubrecht.eu)).

#### Materials availability

This study did not generate new unique reagents.

#### Data and code availability

Read-level bulk and scRNA-seq data of this study have been deposited in Dryad (<https://doi.org/10.5061/dryad.n02v6wx63>) and will be publicly available as of the date of publication. scRNA-seq data from previous publications that were used in this study can be found in Cao et al.,<sup>16</sup> Ma et al.,<sup>36</sup> and The Tabula Sapiens Consortium<sup>71</sup> (see [key resources table](#)). This paper does not report original code. All data were analyzed with commonly used open-source software programs and packages as listed in the [key resources table](#). All bioinformatic processing pipelines are open-source and freely accessible via GitHub at <https://github.com/IARCBioinfo/>.

For any additional information required to reanalyze the data reported in this paper, please contact the [lead contact](#).

### ACKNOWLEDGMENTS

The authors are grateful to the women donating tissue for research. We also thank the team approaching patients for consent. A.A.-R. was also supported by an EMBO long-term fellowship (ALTF-332-2018). We thank Stefan van der Elst and Reinier van der Linden for FACS assistance and Tessa Doelman and Juri Juksar for providing reagents.

### AUTHOR CONTRIBUTIONS

A.A.-R. and H.C. conceived and designed the study. A.A.-R. designed and carried out all the core experiments and analyzed the data. K.G. performed related experiments. M.V. assisted with library preparation. F.S. and A.v.O. provided expertise regarding scRNA-seq library preparation. S.v.d.B. produced and provided tissue culture reagents and Rspodin1 condition medium. S.M.C.d.S.L., F.C., and E.J.P.d.K. provided human fetal pancreas tissue. M.H.G. provided reagents. J.K. and H.B. embedded organoids, cut sections, and performed IHC staining. C.L.-I. and P.J.P. performed TEM of organoids and assisted with the analysis. A.A. provided expertise and conceptual advice about scRNA-seq analysis. J.B., J.v.E., and H.G. provided intellectual input to the study. J.v.E. performed project administration. H.C., J.v.E., and A.A.-R. acquired funding. A.A.-R. (first draft, review, and editing) and H.C. (review and editing) wrote the manuscript. All authors read and approved the manuscript.

### DECLARATION OF INTERESTS

H.C. is an inventor on patents held by the Royal Netherlands Academy of Arts and Sciences that cover organoid technology and a co-founder of Xilis, Duke University (NC). He is currently Head of pharma Research and Early Development (pRED) at Roche, Basel, Switzerland. H.C.'s full disclosure is given at <https://www.uu.nl/staff/JCClevers/>.

### STAR★METHODS

Detailed methods are provided in the online version of this paper and include the following:

- [KEY RESOURCES TABLE](#)
- [EXPERIMENTAL MODEL AND STUDY PARTICIPANT DETAILS](#)
- [METHOD DETAILS](#)
  - Derivation and maintenance of hfPOs and haPOs
  - Growth Rate Analysis
  - Yield determination
  - Morphological purity determination
  - Outgrowth efficiency
  - Differentiation of hfPOs
  - Cell type quantification
  - Enzyme activity sample collection and assays
  - CRISPR organoid reporter-line generation
  - Establishment of clonal lines, DNA extraction and Genotyping of Genetically Engineered Organoids
  - Immunohistochemistry (IHC)
  - Immunofluorescence (IF) and confocal microscopy
  - Transmission electron microscopy (TEM)
  - CryoEM immunogold
  - RNA extraction, quantification and quality control
  - RT-qPCR
  - Bulk RNA-seq analysis
  - Flow cytometry and cell sorting
  - Single-cell derived clonal organoid lines
  - Single-cell transcriptome sample preparation
  - scRNA-seq analysis
- [QUANTIFICATION AND STATISTICAL ANALYSIS](#)

SUPPLEMENTAL INFORMATION

Supplemental information can be found online at <https://doi.org/10.1016/j.cell.2024.10.044>.

Received: April 15, 2024  
Revised: September 18, 2024  
Accepted: October 18, 2024  
Published: December 2, 2024

REFERENCES

- Pan, F.C., and Wright, C. (2011). Pancreas organogenesis: from bud to plexus to gland. *Dev. Dyn.* 240, 530–565. <https://doi.org/10.1002/dvdy.22584>.
- Gannon, M., Herrera, P.L., and Wright, C.V. (2000). Mosaic Cre-mediated recombination in pancreas using the pdx-1 enhancer/promoter. *Genesis* 26, 143–144. [https://doi.org/10.1002/\(sici\)1526-968x\(200002\)26:2<143::aid-gene13>3.0.co;2-l](https://doi.org/10.1002/(sici)1526-968x(200002)26:2<143::aid-gene13>3.0.co;2-l).
- Herrera, P.L. (2000). Adult insulin- and glucagon-producing cells differentiate from two independent cell lineages. *Development* 127, 2317–2322. <https://doi.org/10.1242/dev.127.11.2317>.
- Offield, M.F., Jetton, T.L., Labosky, P.A., Ray, M., Stein, R.W., Magnuson, M.A., Hogan, B.L., and Wright, C.V. (1996). PDX-1 is required for pancreatic outgrowth and differentiation of the rostral duodenum. *Development* 122, 983–995. <https://doi.org/10.1242/dev.122.3.983>.
- Jonsson, J., Carlsson, L., Edlund, T., and Edlund, H. (1994). Insulin-promoter-factor 1 is required for pancreas development in mice. *Nature* 371, 606–609. <https://doi.org/10.1038/371606a0>.
- Kopinke, D., Brailsford, M., Shea, J.E., Leavitt, R., Scaife, C.L., and Murtaugh, L.C. (2011). Lineage tracing reveals the dynamic contribution of Hes1+ cells to the developing and adult pancreas. *Development* 138, 431–441. <https://doi.org/10.1242/dev.053843>.
- Greggio, C., De Franceschi, F., Figueiredo-Larsen, M., Gobaa, S., Ranga, A., Semb, H., Lutolf, M., and Grapin-Botton, A. (2013). Artificial three-dimensional niches deconstruct pancreas development in vitro. *Development* 140, 4452–4462. <https://doi.org/10.1242/dev.096628>.
- Sugiyama, T., Benitez, C.M., Ghodasara, A., Liu, L., McLean, G.W., Lee, J., Blauwkamp, T.A., Nusse, R., Wright, C.V.E., Gu, G., et al. (2013). Reconstituting pancreas development from purified progenitor cells reveals genes essential for islet differentiation. *Proc. Natl. Acad. Sci. USA* 110, 12691–12696. <https://doi.org/10.1073/pnas.1304507110>.
- Jin, L., Feng, T., Shih, H.P., Zerda, R., Luo, A., Hsu, J., Mahdavi, A., Sander, M., Tirrell, D.A., Riggs, A.D., et al. (2013). Colony-forming cells in the adult mouse pancreas are expandable in Matrigel and form endocrine/acinar colonies in laminin hydrogel. *Proc. Natl. Acad. Sci. USA* 110, 3907–3912. <https://doi.org/10.1073/pnas.1301889110>.
- Jin, L., Feng, T., Zerda, R., Chen, C.-C., Riggs, A.D., and Ku, H.T. (2014). In vitro multilineage differentiation and self-renewal of single pancreatic colony-forming cells from adult C57BL/6 mice. *Stem Cells Dev.* 23, 899–909. <https://doi.org/10.1089/scd.2013.0466>.
- Brissova, M., Fowler, M.J., Nicholson, W.E., Chu, A., Hirshberg, B., Harlan, D.M., and Powers, A.C. (2005). Assessment of human pancreatic islet architecture and composition by laser scanning confocal microscopy. *J. Histochem. Cytochem.* 53, 1087–1097. <https://doi.org/10.1369/jhc.5C6684.2005>.
- Scharfmann, R., Xiao, X., Heimberg, H., Mallet, J., and Ravassard, P. (2008). Beta cells within single human islets originate from multiple progenitors. *PLoS One* 3, e3559. <https://doi.org/10.1371/journal.pone.0003559>.
- Chia, C.Y., Madrigal, P., Denil, S.L.I.J., Martinez, I., Garcia-Bernardo, J., El-Khairi, R., Chhatrivala, M., Shepherd, M.H., Hattersley, A.T., Dunn, N.R., et al. (2019). GATA6 cooperates with EOMES/SMAD2/3 to deploy the gene regulatory network governing human definitive endoderm and pancreas formation. *Stem Cell Rep.* 12, 57–70. <https://doi.org/10.1016/j.stemcr.2018.12.003>.
- Jennings, R.E., Berry, A.A., Kirkwood-Wilson, R., Roberts, N.A., Hearn, T., Salisbury, R.J., Blaylock, J., Piper Hanley, K., and Hanley, N.A. (2013). Development of the human pancreas from foregut to endocrine commitment. *Diabetes* 62, 3514–3522. <https://doi.org/10.2337/db12-1479>.
- Piper, K., Brickwood, S., Turnpenney, L.W., Cameron, I.T., Ball, S.G., Wilson, D.I., and Hanley, N.A. (2004). Beta cell differentiation during early human pancreas development. *J. Endocrinol.* 181, 11–23. <https://doi.org/10.1677/joe.0.1810011>.
- Cao, J., O'Day, D.R., Pliner, H.A., Kingsley, P.D., Deng, M., Daza, R.M., Zager, M.A., Aldinger, K.A., Blecher-Gonen, R., Zhang, F., et al. (2020). A human cell atlas of fetal gene expression. *Science* 370, eaba7721. <https://doi.org/10.1126/science.aba7721>.
- Gonçalves, C.A., Larsen, M., Jung, S., Stratmann, J., Nakamura, A., Leuschner, M., Hersemann, L., Keshara, R., Perlman, S., Lundvall, L., et al. (2021). A 3D system to model human pancreas development and its reference single-cell transcriptome atlas identify signaling pathways required for progenitor expansion. *Nat. Commun.* 12, 3144. <https://doi.org/10.1038/s41467-021-23295-6>.
- Yu, X.-X., Qiu, W.-L., Yang, L., Wang, Y.-C., He, M.-Y., Wang, D., Zhang, Y., Li, L.-C., Zhang, J., Wang, Y., et al. (2021). Sequential progenitor states mark the generation of pancreatic endocrine lineages in mice and humans. *Cell Res.* 31, 886–903. <https://doi.org/10.1038/s41422-021-00486-w>.
- Sean, la O., D., Liu, Z., Sun, H., Yu, S.K., Wong, D.M., Chu, E., Rao, S.A., Eng, N., Peixoto, G., et al. (2022). Single-cell multi-omic roadmap of human fetal pancreatic development. Preprint at bioRxiv. <https://doi.org/10.1101/2022.02.17.480942>.
- Pagliuca, F.W., Millman, J.R., Gürtler, M., Segel, M., Van Dervort, A., Ryu, J.H., Peterson, Q.P., Greiner, D., and Melton, D.A. (2014). Generation of functional human pancreatic  $\beta$  cells in vitro. *Cell* 159, 428–439. <https://doi.org/10.1016/j.cell.2014.09.040>.
- Rezania, A., Bruin, J.E., Arora, P., Rubin, A., Batushansky, I., Asadi, A., O'Dwyer, S., Quiskamp, N., Mojibian, M., Albrecht, T., et al. (2014). Reversal of diabetes with insulin-producing cells derived in vitro from human pluripotent stem cells. *Nat. Biotechnol.* 32, 1121–1133. <https://doi.org/10.1038/nbt.3033>.
- Velazco-Cruz, L., Song, J., Maxwell, K.G., Goedegebuure, M.M., Augsornworawat, P., Hoglebe, N.J., and Millman, J.R. (2019). Acquisition of dynamic function in human stem cell-derived  $\beta$  cells. *Stem Cell Rep.* 12, 351–365. <https://doi.org/10.1016/j.stemcr.2018.12.012>.
- Hoglebe, N.J., Augsornworawat, P., Maxwell, K.G., Velazco-Cruz, L., and Millman, J.R. (2020). Targeting the cytoskeleton to direct pancreatic differentiation of human pluripotent stem cells. *Nat. Biotechnol.* 38, 460–470. <https://doi.org/10.1038/s41587-020-0430-6>.
- Mahaddalkar, P.U., Scheibner, K., Pfluger, S., Ansarullah, S., Sterr, M., Beckenbauer, J., Irmeler, M., Beckers, J., Knöbel, S., and Lickert, H. (2020). Generation of pancreatic  $\beta$  cells from CD177+ anterior definitive endoderm. *Nat. Biotechnol.* 38, 1061–1072. <https://doi.org/10.1038/s41587-020-0492-5>.
- Balboa, D., Barsby, T., Lithovius, V., Saarimäki-Vire, J., Omar-Hmeadi, M., Dyachok, O., Montaser, H., Lund, P.-E., Yang, M., Ibrahim, H., et al. (2022). Functional, metabolic and transcriptional maturation of human pancreatic islets derived from stem cells. *Nat. Biotechnol.* 40, 1042–1055. <https://doi.org/10.1038/s41587-022-01219-z>.
- Clevers, H. (2016). Modeling development and disease with organoids. *Cell* 165, 1586–1597. <https://doi.org/10.1016/j.cell.2016.05.082>.
- Kim, J., Koo, B.-K., and Knoblich, J.A. (2020). Human organoids: model systems for human biology and medicine. *Nat. Rev. Mol. Cell Biol.* 21, 571–584. <https://doi.org/10.1038/s41580-020-0259-3>.
- Collombat, P., Xu, X., Ravassard, P., Sosa-Pineda, B., Dussaud, S., Billerstrup, N., Madsen, O.D., Serup, P., Heimberg, H., and Mansouri, A.

- (2009). The ectopic expression of Pax4 in the mouse pancreas converts progenitor cells into alpha and subsequently beta cells. *Cell* 138, 449–462. <https://doi.org/10.1016/j.cell.2009.05.035>.
29. Thorel, F., Népote, V., Avril, I., Kohno, K., Desgraz, R., Chera, S., and Herrera, P.L. (2010). Conversion of adult pancreatic  $\alpha$ -cells to B-cells after extreme B-cell loss. *Nature* 464, 1149–1154. <https://doi.org/10.1038/nature08894>.
  30. Fontcuberta-PiSunyer, M., García-Alamán, A., Prades, È., Téllez, N., Alves-Figueiredo, H., Ramos-Rodríguez, M., Enrich, C., Fernandez-Ruiz, R., Cervantes, S., Clua, L., et al. (2023). Direct reprogramming of human fibroblasts into insulin-producing cells using transcription factors. *Commun. Biol.* 6, 256. <https://doi.org/10.1038/s42003-023-04627-2>.
  31. Chen, Y.-J., Finkbeiner, S.R., Weinblatt, D., Emmett, M.J., Tameire, F., Yousefi, M., Yang, C., Maehr, R., Zhou, Q., Shemer, R., et al. (2014). De novo formation of insulin-producing 'neo- $\beta$  cell islets' from intestinal crypts. *Cell Rep.* 6, 1046–1058. <https://doi.org/10.1016/j.celrep.2014.02.013>.
  32. Li, W.-C., Horb, M.E., Tosh, D., and Slack, J.M.W. (2005). In vitro trans-differentiation of hepatoma cells into functional pancreatic cells. *Mech. Dev.* 122, 835–847. <https://doi.org/10.1016/j.mod.2005.01.001>.
  33. Sumazaki, R., Shiojiri, N., Isoyama, S., Masu, M., Keino-Masu, K., Osawa, M., Nakauchi, H., Kageyama, R., and Matsui, A. (2004). Conversion of biliary system to pancreatic tissue in Hes1-deficient mice. *Nat. Genet.* 36, 83–87. <https://doi.org/10.1038/ng1273>.
  34. Coad, R.A., Dutton, J.R., Tosh, D., and Slack, J.M.W. (2009). Inhibition of Hes1 activity in gall bladder epithelial cells promotes insulin expression and glucose responsiveness. *Biochem. Cell Biol.* 87, 975–987. <https://doi.org/10.1139/o09-063>.
  35. Liu, H., Li, R., Liao, H.-K., Min, Z., Wang, C., Yu, Y., Shi, L., Dan, J., Hayek, A., Martinez Martinez, L., et al. (2021). Chemical combinations potentiate human pluripotent stem cell-derived 3D pancreatic progenitor clusters toward functional  $\beta$  cells. *Nat. Commun.* 12, 3330. <https://doi.org/10.1038/s41467-021-23525-x>.
  36. Ma, X., Lu, Y., Zhou, Z., Li, Q., Chen, X., Wang, W., Jin, Y., Hu, Z., Chen, G., Deng, Q., et al. (2022). Human expandable pancreatic progenitor-derived  $\beta$  cells ameliorate diabetes. *Sci. Adv.* 8, eabk1826. <https://doi.org/10.1126/sciadv.abk1826>.
  37. Zhu, S., Russ, H.A., Wang, X., Zhang, M., Ma, T., Xu, T., Tang, S., Hebrok, M., and Ding, S. (2016). Human pancreatic beta-like cells converted from fibroblasts. *Nat. Commun.* 7, 10080. <https://doi.org/10.1038/ncomms10080>.
  38. Nair, G.G., Liu, J.S., Russ, H.A., Tran, S., Saxton, M.S., Chen, R., Juang, C., Li, M.-L., Nguyen, V.Q., Giacometti, S., et al. (2019). Recapitulating endocrine cell clustering in culture promotes maturation of human stem-cell-derived  $\beta$  cells. *Nat. Cell Biol.* 21, 263–274. <https://doi.org/10.1038/s41556-018-0271-4>.
  39. Boj, S.F., Hwang, C.-I., Baker, L.A., Chio, I.I.C., Engle, D.D., Corbo, V., Jager, M., Ponz-Sarville, M., Tiriach, H., Spector, M.S., et al. (2015). Organoid models of human and mouse ductal pancreatic cancer. *Cell* 160, 324–338. <https://doi.org/10.1016/j.cell.2014.12.021>.
  40. Huch, M., Bonfanti, P., Boj, S.F., Sato, T., Loomans, C.J.M., van de Wetering, M., Sojoodi, M., Li, V.S.W., Schuijers, J., Gracanin, A., et al. (2013). Unlimited in vitro expansion of adult bi-potent pancreas progenitors through the Lgr5/R-spondin axis. *EMBO J.* 32, 2708–2721. <https://doi.org/10.1038/emboj.2013.204>.
  41. Wang, D., Wang, J., Bai, L., Pan, H., Feng, H., Clevers, H., and Zeng, Y.A. (2020). Long-term expansion of pancreatic islet organoids from resident Procr+ progenitors. *Cell* 180, 1198–1211.e19. <https://doi.org/10.1016/j.cell.2020.02.048>.
  42. Loomans, C.J.M., Williams Giuliani, N., Balak, J., Ringnalda, F., van Gurp, L., Huch, M., Boj, S.F., Sato, T., Kester, L., de Sousa Lopes, S.M.C., et al. (2018). Expansion of adult human pancreatic tissue yields organoids harboring progenitor cells with endocrine differentiation potential. *Stem Cell Rep.* 10, 712–724. <https://doi.org/10.1016/j.stemcr.2018.02.005>.
  43. Bonfanti, P., Nobecourt, E., Oshima, M., Albagli-Curiel, O., Laurysens, V., Stangé, G., Sojoodi, M., Heremans, Y., Heimberg, H., and Scharfmann, R. (2015). Ex vivo expansion and differentiation of human and mouse fetal pancreatic progenitors are modulated by epidermal growth factor. *Stem Cells Dev.* 24, 1766–1778. <https://doi.org/10.1089/scd.2014.0550>.
  44. Dominguez-Bendala, J., Qadir, M.M.F., and Pastori, R.L. (2019). Pancreatic progenitors: there and back again. *Trends Endocrinol. Metab.* 30, 4–11. <https://doi.org/10.1016/j.tem.2018.10.002>.
  45. Jiang, F.-X., and Morahan, G. (2015). Multipotent pancreas progenitors: inconclusive but pivotal topic. *World J. Stem Cells* 7, 1251–1261. <https://doi.org/10.4252/wjsc.v7.i11.1251>.
  46. Marty-Santos, L., and Cleaver, O. (2015). Progenitor epithelium: sorting out pancreatic lineages. *J. Histochem. Cytochem.* 63, 559–574. <https://doi.org/10.1369/0022155415586441>.
  47. De Lisle, R.C., and Logsdon, C.D. (1990). Pancreatic acinar cells in culture: expression of acinar and ductal antigens in a growth-related manner. *Eur. J. Cell Biol.* 51, 64–75.
  48. Baldan, J., Houbracken, I., Rومان, I., and Bouwens, L. (2019). Adult human pancreatic acinar cells dedifferentiate into an embryonic progenitor-like state in 3D suspension culture. *Sci. Rep.* 9, 4040. <https://doi.org/10.1038/s41598-019-40481-1>.
  49. Means, A.L., Meszoely, I.M., Suzuki, K., Miyamoto, Y., Rustgi, A.K., Coffey, R.J., Jr., Wright, C.V.E., Stoffers, D.A., and Leach, S.D. (2005). Pancreatic epithelial plasticity mediated by acinar cell transdifferentiation and generation of nestin-positive intermediates. *Development* 132, 3767–3776. <https://doi.org/10.1242/dev.01925>.
  50. Huang, L., Desai, R., Conrad, D.N., Leite, N.C., Akshinthala, D., Lim, C.M., Gonzalez, R., Muthuswamy, L.B., Gartner, Z., and Muthuswamy, S.K. (2021). Commitment and oncogene-induced plasticity of human stem cell-derived pancreatic acinar and ductal organoids. *Cell Stem Cell* 28, 1090–1104.e6. <https://doi.org/10.1016/j.stem.2021.03.022>.
  51. Schmid-Burgk, J.L., Höning, K., Ebert, T.S., and Hornung, V. (2016). CRISPaint allows modular base-specific gene tagging using a ligase-4-dependent mechanism. *Nat. Commun.* 7, 12338. <https://doi.org/10.1038/ncomms12338>.
  52. Artegiani, B., Hendriks, D., Beumer, J., Kok, R., Zheng, X., Joore, I., Chua de Sousa Lopes, S., van Zon, J., Tans, S., and Clevers, H. (2020). Fast and efficient generation of knock-in human organoids using homology-independent CRISPR-Cas9 precision genome editing. *Nat. Cell Biol.* 22, 321–331. <https://doi.org/10.1038/s41556-020-0472-5>.
  53. Histology Guide <https://histologyguide.com/>.
  54. Lugea, A., Waldron, R.T., Mareninova, O.A., Shalbuva, N., Deng, N., Su, H.-Y., Thomas, D.D., Jones, E.K., Messenger, S.W., Yang, J., et al. (2017). Human Pancreatic Acinar Cells: proteomic Characterization, Physiologic Responses, and organellar Disorders in ex vivo Pancreatitis. *Am. J. Pathol.* 187, 2726–2743. <https://doi.org/10.1016/j.ajpath.2017.08.017>.
  55. Krapp, A., Knöfler, M., Ledermann, B., Bürki, K., Berney, C., Zoerkler, N., Hagenbüchle, O., and Wellauer, P.K. (1998). The bHLH protein PTF1-p48 is essential for the formation of the exocrine and the correct spatial organization of the endocrine pancreas. *Genes Dev.* 12, 3752–3763. <https://doi.org/10.1101/gad.12.23.3752>.
  56. Masui, T., Swift, G.H., Deering, T., Shen, C., Coats, W.S., Long, Q., Elsäßer, H.-P., Magnuson, M.A., and MacDonald, R.J. (2010). Replacement of Rbpj with Rbpjl in the PTF1 complex controls the final maturation of pancreatic acinar cells. *Gastroenterology* 139, 270–280. <https://doi.org/10.1053/j.gastro.2010.04.003>.
  57. Krah, N.M., De La O, J.-P., Swift, G.H., Hoang, C.Q., Willet, S.G., Chen Pan, F., Cash, G.M., Bronner, M.P., Wright, C.V., MacDonald, R.J., et al. (2015). The acinar differentiation determinant PTF1A inhibits

- initiation of pancreatic ductal adenocarcinoma. *eLife* 4, e07125. <https://doi.org/10.7554/eLife.07125>.
58. Millman, J.R., Xie, C., Van Dervort, A., Gürtler, M., Pagliuca, F.W., and Melton, D.A. (2016). Generation of stem cell-derived  $\beta$ -cells from patients with type 1 diabetes. *Nat. Commun.* 7, 11463. <https://doi.org/10.1038/ncomms11463>.
  59. Bocian-Sobkowska, J., Zabel, M., Wozniak, W., and Surdyk-Zasada, J. (1999). Polyhormonal aspect of the endocrine cells of the human fetal pancreas. *Histochem. Cell Biol.* 112, 147–153. <https://doi.org/10.1007/s004180050401>.
  60. Gradwohl, G., Dierich, A., LeMeur, M., and Guillemot, F. (2000). Neurogenin3 is required for the development of the four endocrine cell lineages of the pancreas. *Proc. Natl. Acad. Sci. USA* 97, 1607–1611. <https://doi.org/10.1073/pnas.97.4.1607>.
  61. Zhao, Z., Chen, X., Dowbaj, A.M., Sijukic, A., Bratlie, K., Lin, L., Fong, E.L.S., Balachander, G.M., Chen, Z., Soragni, A., et al. (2022). Organoids. *Nat. Rev. Methods Primers* 2, 94. <https://doi.org/10.1038/s43586-022-00174-y>.
  62. Salmen, F., De Jonghe, J., Kaminski, T.S., Alemany, A., Parada, G.E., Verity-Legg, J., Yanagida, A., Kohler, T.N., Battich, N., van den Brekel, F., et al. (2022). High-throughput total RNA sequencing in single cells using VASA-seq. *Nat. Biotechnol.* 40, 1780–1793. <https://doi.org/10.1038/s41587-022-01361-8>.
  63. Bergen, V., Lange, M., Peidli, S., Wolf, F.A., and Theis, F.J. (2020). Generalizing RNA velocity to transient cell states through dynamical modeling. *Nat. Biotechnol.* 38, 1408–1414. <https://doi.org/10.1038/s41587-020-0591-3>.
  64. Villani, V., Thornton, M.E., Zook, H.N., Crook, C.J., Grubbs, B.H., Orlando, G., De Filippo, R., Ku, H.T., and Perin, L. (2019). SOX9+PTF1A+ Cells Define the Tip Progenitor Cells of the Human Fetal Pancreas of the Second Trimester. *Stem Cells Transl. Med.* 8, 1249–1264. <https://doi.org/10.1002/sctm.19-0231>.
  65. Ramond, C., Glaser, N., Berthault, C., Ameri, J., Kirkegaard, J.S., Hansson, M., Honoré, C., Semb, H., and Scharfmann, R. (2017). Reconstructing human pancreatic differentiation by mapping specific cell populations during development. *eLife* 6, e27564. <https://doi.org/10.7554/eLife.27564>.
  66. Rindler, M.J., and Hoops, T.C. (1990). The pancreatic membrane protein GP-2 localizes specifically to secretory granules and is shed into the pancreatic juice as a protein aggregate. *Eur. J. Cell Biol.* 53, 154–163.
  67. Decker, K., Goldman, D.C., Grasch, C.L., and Sussel, L. (2006). Gata6 is an important regulator of mouse pancreas development. *Dev. Biol.* 298, 415–429. <https://doi.org/10.1016/j.ydbio.2006.06.046>.
  68. Rovira, M., Delaspre, F., Massumi, M., Serra, S.A., Valverde, M.A., Lloreta, J., Dufresne, M., Payré, B., Konieczny, S.F., Savatier, P., et al. (2008). Murine embryonic stem cell-derived pancreatic acinar cells recapitulate features of early pancreatic differentiation. *Gastroenterology* 135, 1301–1310. <https://doi.org/10.1053/j.gastro.2008.06.049>.
  69. Grapin-Botton, A. (2005). Ductal cells of the pancreas. *Int. J. Biochem. Cell Biol.* 37, 504–510. <https://doi.org/10.1016/j.biocel.2004.07.010>.
  70. Olaniru, O.E., Kadolsky, U., Kannambath, S., Vaikinen, H., Fung, K., Dhimi, P., and Persaud, S.J. (2023). Single-cell transcriptomic and spatial landscapes of the developing human pancreas. *Cell Metab.* 35, 184–199.e5. <https://doi.org/10.1016/j.cmet.2022.11.009>.
  71. Tabula Sapiens Consortium\*, Jones, R.C., Karkanas, J., Krasnow, M.A., Pisco, A.O., Quake, S.R., Salzman, J., Yosef, N., Bulthaupt, B., Brown, P., et al. (2022). The Tabula Sapiens: a multiple-organ, single-cell transcriptomic atlas of humans. *Science* 376, eab4896. <https://doi.org/10.1126/science.ab4896>.
  72. Qadir, M.M.F., Álvarez-Cubela, S., Klein, D., van Dijk, J., Muñoz-Anquela, R., Moreno-Hernández, Y.B., Lanzoni, G., Sadiq, S., Navarro-Rubio, B., García, M.T., et al. (2020). Single-cell resolution analysis of the human pancreatic ductal progenitor cell niche. *Proc. Natl. Acad. Sci. USA* 117, 10876–10887. <https://doi.org/10.1073/pnas.1918314117>.
  73. Hrvatin, S., O'Donnell, C.W., Deng, F., Millman, J.R., Pagliuca, F.W., Dilorio, P., Rezania, A., Gifford, D.K., and Melton, D.A. (2014). Differentiated human stem cells resemble fetal, not adult,  $\beta$  cells. *Proc. Natl. Acad. Sci. USA* 111, 3038–3043. <https://doi.org/10.1073/pnas.1400709111>.
  74. Veres, A., Faust, A.L., Bushnell, H.L., Engquist, E.N., Kenty, J.H.-R., Harb, G., Poh, Y.-C., Sintov, E., Gürtler, M., Pagliuca, F.W., et al. (2019). Charting cellular identity during human in vitro  $\beta$ -cell differentiation. *Nature* 569, 368–373. <https://doi.org/10.1038/s41586-019-1168-5>.
  75. Muraro, M.J., Dharmadhikari, G., Grün, D., Groen, N., Dielen, T., Jansen, E., van Gorp, L., Engelse, M.A., Carlotti, F., de Koning, E.J.P., et al. (2016). A single-cell transcriptome atlas of the human pancreas. *Cell Syst.* 3, 385–394.e3. <https://doi.org/10.1016/j.cels.2016.09.002>.
  76. Yin, L., Li, Y., Ren, J., Kuwahara, H., and Kufe, D. (2003). Human MUC1 carcinoma antigen regulates intracellular oxidant levels and the apoptotic response to oxidative stress. *J. Biol. Chem.* 278, 35458–35464. <https://doi.org/10.1074/jbc.M301987200>.
  77. Ringel, J., and Löhr, M. (2003). The MUC gene family: their role in diagnosis and early detection of pancreatic cancer. *Mol. Cancer* 2, 9. <https://doi.org/10.1186/1476-4598-2-9>.
  78. Bruin, J.E., Erener, S., Vela, J., Hu, X., Johnson, J.D., Kurata, H.T., Lynn, F.C., Piret, J.M., Asadi, A., Rezania, A., et al. (2014). Characterization of polyhormonal insulin-producing cells derived in vitro from human embryonic stem cells. *Stem Cell Res.* 12, 194–208. <https://doi.org/10.1016/j.scr.2013.10.003>.
  79. La Manno, G., Soldatov, R., Zeisel, A., Braun, E., Hochgerner, H., Petukhov, V., Lidschreiber, K., Kastrioti, M.E., Lönnerberg, P., Furlan, A., et al. (2018). RNA velocity of single cells. *Nature* 560, 494–498. <https://doi.org/10.1038/s41586-018-0414-6>.
  80. Barker, N., van Es, J.H., Kuipers, J., Kujala, P., van den Born, M., Cozijnsen, M., Haegebarth, A., Korving, J., Begthel, H., Peters, P.J., et al. (2007). Identification of stem cells in small intestine and colon by marker gene Lgr5. *Nature* 449, 1003–1007. <https://doi.org/10.1038/nature06196>.
  81. Muñoz, J., Stange, D.E., Schepers, A.G., van de Wetering, M., Koo, B.-K., Itzkovitz, S., Volckmann, R., Kung, K.S., Koster, J., Radulescu, S., et al. (2012). The Lgr5 intestinal stem cell signature: robust expression of proposed quiescent ‘+4’ cell markers. *EMBO J.* 31, 3079–3091. <https://doi.org/10.1038/emboj.2012.166>.
  82. Jin, L., Gao, D., Feng, T., Tremblay, J.R., Ghazalli, N., Luo, A., Rawson, J., Quijano, J.C., Chai, J., Wedeken, L., et al. (2016). Cells with surface expression of CD133<sup>high</sup>CD71<sup>low</sup> are enriched for tripotent colony-forming progenitor cells in the adult murine pancreas. *Stem Cell Res.* 16, 40–53. <https://doi.org/10.1016/j.scr.2015.11.015>.
  83. Cogger, K.F., Sinha, A., Sarangi, F., McGaugh, E.C., Saunders, D., Dorell, C., Mejia-Guerrero, S., Aghazadeh, Y., Rourke, J.L., Sreaton, R.A., et al. (2017). Glycoprotein 2 is a specific cell surface marker of human pancreatic progenitors. *Nat. Commun.* 8, 331. <https://doi.org/10.1038/s41467-017-00561-0>.
  84. Aghazadeh, Y., Sarangi, F., Poon, F., Nkenkor, B., McGaugh, E.C., Nunes, S.S., and Nostro, M.C. (2022). GP2-enriched pancreatic progenitors give rise to functional beta cells in vivo and eliminate the risk of teratoma formation. *Stem Cell Rep.* 17, 964–978. <https://doi.org/10.1016/j.stemcr.2022.03.004>.
  85. De Vas, M.G., Kopp, J.L., Heliot, C., Sander, M., Cereghini, S., and Haudmair, C. (2015). Hnf1b controls pancreas morphogenesis and the generation of Ngn3+ endocrine progenitors. *Development* 142, 871–882. <https://doi.org/10.1242/dev.110759>.
  86. Seymour, P.A., Freude, K.K., Tran, M.N., Mayes, E.E., Jensen, J., Kist, R., Scherer, G., and Sander, M. (2007). SOX9 is required for maintenance of the pancreatic progenitor cell pool. *Proc. Natl. Acad. Sci. USA* 104, 1865–1870. <https://doi.org/10.1073/pnas.0609217104>.

87. Kopp, J.L., Dubois, C.L., Schaffer, A.E., Hao, E., Shih, H.P., Seymour, P.A., Ma, J., and Sander, M. (2011). Sox9<sup>+</sup> ductal cells are multipotent progenitors throughout development but do not produce new endocrine cells in the normal or injured adult pancreas. *Development* *138*, 653–665. <https://doi.org/10.1242/dev.056499>.
88. Jensen, K.B., Collins, C.A., Nascimento, E., Tan, D.W., Frye, M., Itami, S., and Watt, F.M. (2009). Lrig1 expression defines a distinct multipotent stem cell population in mammalian epidermis. *Cell Stem Cell* *4*, 427–439. <https://doi.org/10.1016/j.stem.2009.04.014>.
89. Koo, B.-K., Spit, M., Jordens, I., Low, T.Y., Stange, D.E., van de Wetering, M., van Es, J.H., Mohammed, S., Heck, A.J.R., Maurice, M.M., et al. (2012). Tumour suppressor RNF43 is a stem-cell E3 ligase that induces endocytosis of Wnt receptors. *Nature* *488*, 665–669. <https://doi.org/10.1038/nature11308>.
90. Hao, H.-X., Xie, Y., Zhang, Y., Charlat, O., Oster, E., Avello, M., Lei, H., Mickanin, C., Liu, D., Ruffner, H., et al. (2012). ZNRF3 promotes Wnt receptor turnover in an R-spondin-sensitive manner. *Nature* *485*, 195–200. <https://doi.org/10.1038/nature11019>.
91. Stange, D.E., Koo, B.-K., Huch, M., Sibbel, G., Basak, O., Lyubimova, A., Kujala, P., Bartfeld, S., Koster, J., Geahlen, J.H., et al. (2013). Differentiated Troy<sup>+</sup> chief cells act as reserve stem cells to generate all lineages of the stomach epithelium. *Cell* *155*, 357–368. <https://doi.org/10.1016/j.cell.2013.09.008>.
92. Pan, F.C., and Brissova, M. (2014). Pancreas development in humans. *Curr. Opin. Endocrinol. Diabetes Obes.* *21*, 77–82. <https://doi.org/10.1097/MED.0000000000000047>.
93. Senger, S., Ingano, L., Freire, R., Anselmo, A., Zhu, W., Sadreyev, R., Walker, W.A., and Fasano, A. (2018). Human fetal-derived enterospheres provide insights on intestinal development and a novel model to study necrotizing enterocolitis (NEC). *Cell. Mol. Gastroenterol. Hepatol.* *5*, 549–568. <https://doi.org/10.1016/j.jcmgh.2018.01.014>.
94. Hu, H., Gehart, H., Artegiani, B., López-Iglesias, C., Dekkers, F., Basak, O., van Es, J., Chuva de Sousa Lopes, S.M., Begthel, H., Korving, J., et al. (2018). Long-term expansion of functional mouse and human hepatocytes as 3D organoids. *Cell* *175*, 1591–1606.e19. <https://doi.org/10.1016/j.cell.2018.11.013>.
95. Liang, J., Qian, J., Yang, L., Chen, X., Wang, X., Lin, X., Wang, X., and Zhao, B. (2022). Modeling human thyroid development by fetal tissue-derived organoid culture. *Adv. Sci. (Weinh)* *9*, e2105568. <https://doi.org/10.1002/advs.202105568>.
96. Roccio, M., Perry, M., Ealy, M., Widmer, H.R., Heller, S., and Senn, P. (2018). Molecular characterization and prospective isolation of human fetal cochlear hair cell progenitors. *Nat. Commun.* *9*, 4027. <https://doi.org/10.1038/s41467-018-06334-7>.
97. Nikolić, M.Z., Caritg, O., Jeng, Q., Johnson, J.-A., Sun, D., Howell, K.J., Brady, J.L., Laresgoiti, U., Allen, G., Butler, R., et al. (2017). Human embryonic lung epithelial tips are multipotent progenitors that can be expanded in vitro as long-term self-renewing organoids. *eLife* *6*, e26575. <https://doi.org/10.7554/eLife.26575>.
98. Fordham, R.P., Yui, S., Hannan, N.R.F., Soendergaard, C., Madgwick, A., Schweiger, P.J., Nielsen, O.H., Vallier, L., Pedersen, R.A., Nakamura, T., et al. (2013). Transplantation of expanded fetal intestinal progenitors contributes to colon regeneration after injury. *Cell Stem Cell* *13*, 734–744. <https://doi.org/10.1016/j.stem.2013.09.015>.
99. Hendriks, D., Pagliaro, A., Andreatta, F., Ma, Z., van Giessen, J., Massalini, S., López-Iglesias, C., van Son, G.J.F., DeMartino, J., Damen, J.M.A., et al. (2024). Human fetal brain self-organizes into long-term expanding organoids. *Cell* *187*, 712–732.e38. <https://doi.org/10.1016/j.cell.2023.12.012>.
100. Laitio, M., Lev, R., and Orlic, D. (1974). The developing human fetal pancreas: an ultrastructural and histochemical study with special reference to exocrine cells. *J. Anat.* *117*, 619–634.
101. Sato, T., Stange, D.E., Ferrante, M., Vries, R.G.J., Van Es, J.H., Van den Brink, S., Van Houdt, W.J., Pronk, A., Van Gorp, J., Siersema, P.D., et al. (2011). Long-term expansion of epithelial organoids from human colon, adenoma, adenocarcinoma, and Barrett's epithelium. *Gastroenterology* *141*, 1762–1772. <https://doi.org/10.1053/j.gastro.2011.07.050>.
102. Basak, O., Krieger, T.G., Muraro, M.J., Wiebrands, K., Stange, D.E., Frias-Aldeguer, J., Rivron, N.C., van de Wetering, M., van Es, J.H., van Oudenaarden, A., et al. (2018). Troy<sup>+</sup> brain stem cells cycle through quiescence and regulate their number by sensing niche occupancy. *Proc. Natl. Acad. Sci. USA* *115*, E610–E619. <https://doi.org/10.1073/pnas.1715911114>.
103. Basak, O., Beumer, J., Wiebrands, K., Seno, H., van Oudenaarden, A., and Clevers, H. (2017). Induced quiescence of Lgr5<sup>+</sup> stem cells in intestinal organoids enables differentiation of hormone-producing enteroendocrine cells. *Cell Stem Cell* *20*, 177–190.e4. <https://doi.org/10.1016/j.stem.2016.11.001>.
104. Beumer, J., Puschhof, J., Bauzá-Martinez, J., Martínez-Silgado, A., Elementaite, R., James, K.R., Ross, A., Hendriks, D., Artegiani, B., Buslinger, G.A., et al. (2020). High-resolution mRNA and secretome atlas of human enteroendocrine cells. *Cell* *181*, 1291–1306.e19. <https://doi.org/10.1016/j.cell.2020.04.036>.
105. Love, M.I., Huber, W., and Anders, S. (2014). Moderated estimation of fold change and dispersion for RNA-seq data with DESeq2. *Genome Biol.* *15*, 550. <https://doi.org/10.1186/s13059-014-0550-8>.
106. Wolf, F.A., Angerer, P., and Theis, F.J. (2018). SCANPY: large-scale single-cell gene expression data analysis. *Genome Biol.* *19*, 15. <https://doi.org/10.1186/s13059-017-1382-0>.
107. Gómez-Rubio, V. (2017). ggplot2 – Elegant Graphics for Data Analysis (2nd Edition). *J. Stat. Soft.* *77*, Ggplot2. <https://doi.org/10.18637/jss.v077.b02>.
108. Gu, Z., Eils, R., and Schlesner, M. (2016). Complex heatmaps reveal patterns and correlations in multidimensional genomic data. *Bioinformatics* *32*, 2847–2849. <https://doi.org/10.1093/bioinformatics/btw313>.
109. Broutier, L., Andersson-Rolf, A., Hindley, C.J., Boj, S.F., Clevers, H., Koo, B.-K., and Huch, M. (2016). Culture and establishment of self-renewing human and mouse adult liver and pancreas 3D organoids and their genetic manipulation. *Nat. Protoc.* *11*, 1724–1743. <https://doi.org/10.1038/nprot.2016.097>.
110. Hogrebe, N.J., Maxwell, K.G., Augsornworawat, P., and Millman, J.R. (2021). Generation of insulin-producing pancreatic  $\beta$  cells from multiple human stem cell lines. *Nat. Protoc.* *16*, 4109–4143. <https://doi.org/10.1038/s41596-021-00560-y>.
111. Peterson, Q.P., Veres, A., Chen, L., Slama, M.Q., Kenty, J.H.R., Hassoun, S., Brown, M.R., Dou, H., Duffy, C.D., Zhou, Q., et al. (2020). A method for the generation of human stem cell-derived alpha cells. *Nat. Commun.* *11*, 2241. <https://doi.org/10.1038/s41467-020-16049-3>.
112. Fujii, M., Matano, M., Nanki, K., and Sato, T. (2015). Efficient genetic engineering of human intestinal organoids using electroporation. *Nat. Protoc.* *10*, 1474–1485. <https://doi.org/10.1038/nprot.2015.088>.
113. Pleguezuelos-Manzano, C., Puschhof, J., van den Brink, S., Geurts, V., Beumer, J., and Clevers, H. (2020). Establishment and culture of human intestinal organoids derived from adult stem cells. *Curr. Protoc. Immunol.* *130*, e106. <https://doi.org/10.1002/cpim.106>.
114. Dobin, A., Davis, C.A., Schlesinger, F., Drenkow, J., Zaleski, C., Jha, S., Batut, P., Chaisson, M., and Gingeras, T.R. (2013). STAR: ultrafast universal RNA-seq aligner. *Bioinformatics* *29*, 15–21. <https://doi.org/10.1093/bioinformatics/bts635>.
115. Martin, M. (2011). Cutadapt removes adapter sequences from high-throughput sequencing reads. *EMBnetjournal* *17*, 10–12. <https://doi.org/10.14806/ej.17.1.200>.
116. Li, H., and Durbin, R. (2009). Fast and accurate short read alignment with Burrows-Wheeler transform. *Bioinformatics* *25*, 1754–1760. <https://doi.org/10.1093/bioinformatics/btp324>.

117. Wolock, S.L., Lopez, R., and Klein, A.M. (2019). Scrublet: computational identification of cell doublets in single-cell transcriptomic data. *Cell Syst.* *8*, 281–291.e9. <https://doi.org/10.1016/j.cels.2018.11.005>.
118. Virshup, I., Rybakov, S., Theis, F.J., Angerer, P., and Alexander Wolf, F. (2021). anndata: annotated data. Preprint at bioRxiv. <https://doi.org/10.1101/2021.12.16.473007>.
119. McInnes, L., Healy, J., and Melville, J. (2018). UMAP: Uniform Manifold Approximation and Projection for Dimension Reduction. *J. Open Source Softw.* *3*, 861.
120. Korsunsky, I., Millard, N., Fan, J., Slowikowski, K., Zhang, F., Wei, K., Baglaenko, Y., Brenner, M., Loh, P.-R., and Raychaudhuri, S. (2019). Fast, sensitive and accurate integration of single-cell data with Harmony. *Nat. Methods* *16*, 1289–1296. <https://doi.org/10.1038/s41592-019-0619-0>.
121. Traag, V., Waltman, L., and van Eck, N.J. (2018). From Louvain to Leiden: guaranteeing well-connected communities. Preprint at arXiv. <https://doi.org/10.48550/arXiv.1810.08473>.
122. Hie, B., Bryson, B., and Berger, B. (2019). Efficient integration of heterogeneous single-cell transcriptomes using Scanorama. *Nat. Biotechnol.* *37*, 685–691. <https://doi.org/10.1038/s41587-019-0113-3>.

## STAR★METHODS

### KEY RESOURCES TABLE

REAGENT or RESOURCE	SOURCE	IDENTIFIER
<b>Antibodies</b>		
Alexa Fluor 488 donkey anti-mouse	Thermo Fisher Scientific	A-21202 RRID:AB_141607
Alexa Fluor 568 donkey anti-rabbit	Thermo Fisher Scientific	A10042 RRID:AB_2534017
Alexa Fluor 647 donkey anti-rat	Thermo Fisher Scientific	A48272 RRID:AB_2893138
Cytokeratin 19 (Ck19)	Cell Signaling	4558 RRID:AB_2133455
insulin (proinsulin; C-peptide)	DSHB	GN-ID4 RRID:AB_2255626
Chromogranin A (C-20)	Santa Cruz	sc-1488 RRID:AB_2276319
Somatostatin	Santa Cruz	sc-74556 RRID:AB_2271061
Carboxypeptidase A	Abcam	ab173283
PRSS1	Thermo Fisher Scientific	PA5-46939; RRID:AB_2609646
CELA3A	Thermo Fisher Scientific	HPA045650; RRID:AB_2679407
Anti-RNASE1	Merck	HPA001140; RRID:AB_1079816
Chymotrypsin	Thermo Fisher Scientific	PA5-83848; RRID:AB_2791000
<b>Biological samples</b>		
Human fetal pancreatic tissues (GW8-GW17)	Leiden University Medical Center and Human Developmental Biology Resource	N/A
Human adult pancreatic tissue	St. Antonius Hospital Nieuwegein, UMC Utrecht	N/A
<b>Chemicals, peptides, and recombinant proteins</b>		
Atto 647N	Sigma-Aldrich	65906
DAPI	Thermo Fisher Scientific	62248
Advanced DMEM/F12	Thermo Fisher Scientific	12634010
Advanced DMEM/F12	Thermo Fisher Scientific	12634010
Penicillin-Streptomycin	Thermo Fisher Scientific	15140122
GlutaMAX	Thermo Fisher Scientific	35050061
HEPES	Thermo Fisher Scientific	15630080
Neurobasal medium	Thermo Fisher Scientific	21103049
B-27 supplement, minus vitamin A	Thermo Fisher Scientific	12587010
B-27 supplement	Thermo Fisher Scientific	17504044
N-2 supplement	Thermo Fisher Scientific	17502048
MEM non-essential amino acid solution	Thermo Fisher Scientific	11140050
Human EGF	Peptotech	AF-100-15
Human FGF-2	Peptotech	100-18B
Human FGF-10	Peptotech	100-26
Primocin	Invivogen	ant-pm-2
Cultrex Basement Membrane Extract (BME), Growth Factor Reduced, Type 2	R and D systems	3533-010-02
Corning Matrigel hESC-Qualified Matrix	Corning	354277
Y-27632 dihydrochloride	AbMole	M1817
KnockOut Serum Replacement	Thermo Fisher Scientific	10828028
Opti-MEM, no Phenol Red	Thermo Fisher Scientific	1105802
Blasticidin	Invivogen	ant-bl-05
Chemically Defined Lipid Concentrate	Thermo Fisher Scientific	11905031
Vitamin C	Sigma-Aldrich	#A92902

(Continued on next page)

**Continued**

REAGENT or RESOURCE	SOURCE	IDENTIFIER
Heparin	Sigma-Aldrich	H4784
10 $\mu$ M Alk5	SCBT	sc-221234B
Retinoic Acid	Sigma-Aldrich	R2625
SANT1	SCBT	sc-203253
3,3',5-Triiodo-L-thyronine sodium salt (T3)	Sigma-Aldrich	T6397
Gamma secretase Inhibitor II (LY411575)	Sigma-Aldrich	SML0649
Dexamethasone	Sigma-Aldrich	D4902
3-Isobutyl-1-methylxanthine (IBMX)	Sigma-Aldrich	I5879
Forskolin	R&D	1099
<b>Critical commercial assays</b>		
iQ SYBR Green Supermix	Bio-Rad	1708886
C-Peptide ELISA	Alpco	80-CPTHU-E01.1
Lipase Assay Kit III (Fluorometric)	ab118969	Abcam
Carbonic Anhydrase (CA) Activity Assay Kit (Colorimetric)	Abcam	ab284550
Human Trypsin 1/PRSS1 ELISA Kit	Raybiotech	ELH-TRYP1-1
<b>Deposited data</b>		
Read-level bulk and single-cell RNA sequencing data generated in this study	This manuscript	Dryad: <a href="https://doi.org/10.5061/dryad.n02v6wx63">https://doi.org/10.5061/dryad.n02v6wx63</a>
Previously published single-cell RNA sequencing data on human fetal pancreas	Cao et al. <sup>16</sup>	GEO: <a href="https://www.ncbi.nlm.nih.gov/geo/query/acc.cgi?acc=GSE156793">https://www.ncbi.nlm.nih.gov/geo/query/acc.cgi?acc=GSE156793</a>
Previously published single-cell RNA sequencing data on human fetal pancreas	Ma et al. <sup>36</sup>	OMIX: <a href="https://bigd.big.ac.cn/omix/(identifier%20OMIX236)">https://bigd.big.ac.cn/omix/(identifier OMIX236)</a>
Previously published single-cell RNA sequencing data on human adult pancreas	The Tabula Sapiens Consortium <sup>71</sup>	GEO: <a href="https://www.ncbi.nlm.nih.gov/geo/query/acc.cgi?acc=GSE201333">https://www.ncbi.nlm.nih.gov/geo/query/acc.cgi?acc=GSE201333</a>
<b>Oligonucleotides</b>		
sgRNA cloning primers, qPCR primers and genotyping primers	See <a href="#">Table S6</a>	This manuscript.
Addgene plasmid	Addgene	#65777
<b>Software and algorithms</b>		
RStudio 2022.02.2	RStudio, PBC	<a href="https://www.rstudio.com/">https://www.rstudio.com/</a>
DESeq2 1.36.0	Love et al. <sup>105</sup>	<a href="https://bioconductor.org/packages/release/bioc/html/DESeq2.html">https://bioconductor.org/packages/release/bioc/html/DESeq2.html</a>
Scanpy	Wolf et al. <sup>106</sup>	<a href="https://pypi.org/project/scanpy/">https://pypi.org/project/scanpy/</a>
scVelo	Bergen et al. <sup>63</sup>	<a href="https://pypi.org/project/scvelo/">https://pypi.org/project/scvelo/</a>
Uniprot human database (Organism Species 9606)	Uniprot	<a href="https://www.uniprot.org/">https://www.uniprot.org/</a>
Las X 3.5.7	Leica	N/A
Fiji 2.14.0	ImageJ	<a href="https://imagej.net/">https://imagej.net/</a>
Prism 9.4.1	GraphPad	<a href="https://www.graphpad.com/">https://www.graphpad.com/</a>
Adobe Illustrator 28.0 and Photoshop 25.1.0	Adobe Inc.	<a href="https://www.adobe.com/">https://www.adobe.com/</a>
GraphPad Prism (v.8.2.0).	GraphPad Software	SCR_002798
ggplot2	ggplot2 - Elegant Graphics for Data Analysis (2nd Edition) <sup>107</sup>	<a href="https://ggplot2.tidyverse.org">https://ggplot2.tidyverse.org</a>
EnhancedVolcano	Blighe K	<a href="https://bioconductor.org/packages/release/bioc/html/EnhancedVolcano.html">https://bioconductor.org/packages/release/bioc/html/EnhancedVolcano.html</a>
ComplexHeatmap	Gu et al. <sup>108</sup>	<a href="https://bioconductor.org/packages/release/bioc/html/ComplexHeatmap.html">https://bioconductor.org/packages/release/bioc/html/ComplexHeatmap.html</a>

(Continued on next page)

**Continued**

REAGENT or RESOURCE	SOURCE	IDENTIFIER
Rstudio	Posit	<a href="https://posit.co/download/rstudio-desktop/">https://posit.co/download/rstudio-desktop/</a>
FlowJo (Tree Star)	BD (Becton, Dickinson & Company)	N/A

**EXPERIMENTAL MODEL AND STUDY PARTICIPANT DETAILS**

Human fetal pancreas tissues were obtained following consent from women who had determined to terminate their pregnancy, and its use for research was approved by the Dutch Ethical Medical Council (Leiden University Medical Centre). In total,  $n = 21$  tissues were used in this study. Tissues were from both genders (5 female, 2 male, and 14 undetermined) and ranged in developmental stage from GW8 to GW17.

Collection of human adult pancreas tissue was performed according to the guidelines of the European Network of Research Ethics Committees (EUREC) following European, national and local law. The protocols were approved by the medical ethical committee (METC) corresponding to the respective hospitals where patients were treated: Verenigde Commissies Mensgebonden Onderzoek of the St. Antonius Hospital Nieuwegein, Z-12.55; UMC Utrecht, METC 12-093 HUB-Cancer; NKI Institutional Review Board (IRB), M18ORG/CFMPB582; Maastricht University Medical Center, METC 2019-1061, and 2019-1039. Human adult pancreatic organoids (haPOs) were established and maintained as previously described.<sup>109</sup>

Sample size estimation was not performed. hfPO lines, within the same morphological group, were randomly assigned to different groups for the experiments. For statistical comparisons differences were significant when  $p < 0.05$ . Information about sample size and statistical tests can be found in the figure legends.

**METHOD DETAILS**

**Derivation and maintenance of hfPOs and haPOs**

In brief, to establish human fetal pancreatic organoid lines (hfPOs), human fetal pancreas tissue was cut into small pieces and then incubated with collagenase type IV (Sigma-Aldrich) for 5min at 37°C followed by manual dissociation by pipetting. The single cell-tissue fragment solution was washed 2 times with AdvDMEM+++ (AdDMEM/F-12 medium supplemented with 1× GlutaMAX, 10 mM HEPES and 100 U ml<sup>-1</sup> penicillin/streptomycin solution (all Thermo Fisher)) and seeded in 100µl of Matrigel (Corning) suspension (3:1 Matrigel:AdvDMEM+++ per well of a 12-well plate (four-five droplets per well (20-25µl per droplet))).

hfPOs were maintained in hfPO medium consisting of AdvDMEM+++ supplemented with 20% RSPO1-conditioned medium (in-house production), 1% Noggin conditioned medium (U-Protein express), 1× B-27 Supplement (Thermo Fisher), 1.25 mM N-acetyl-L-cysteine, 50 ng/ml hEGF, 10 ng/ml hFGF2 (all Peprotech), 500 nM A 83-01, 1 µM PGE2 (Tocris), 5 µM Y-27632 (AbMole) and 50 µg/ml Primocin (InvivoGen). The first days and first passage post establishment, the hfPO medium was supplemented with extra Y-27632 (final concentration, 10 µM) to minimize anoikis. hfPOs were passaged by gentle mechanical disruption by pipetting every 21–35 days at a ratio of 1:3–1:4. During the first few passages, the splitting ratio was 1:1-1:2. For increasing the expression of LGR5 1µM valproic acid (Sigma) and 1µM CHIR (Sigma) was added to the expansion medium.

**Growth Rate Analysis**

Single cells (15000) were plated in 20µl of Matrigel. After three weeks in culture (in expansion hfPO medium), organoids were collected and dissociated into single cells. The number of cells were counted using a cell counter (Denovix) and the total cell number was determined. Counting was performed on four different wells. By calculating the number of cells at day 21, which all came from the 15000 cells plated at day 0, a multiplication factor could be determined for each passage. Using this, a theoretical total number of cells could be calculated by multiplying the total cell number of the previous passage with the multiplication factor of that passage. Subsequently, 15000 of the counted single cells were plated in 20µl Matrigel. This procedure was repeated twice.

**Yield determination**

Single organoids from lines at an early or late passage were manually picked and dissociated into single cell. The number of cells were counted using a cell counter (Denovix).”

**Morphological purity determination**

Single cystic or budding organoids from lines at an early or late passage were manually picked and split. The number of budding and cystic organoids were then quantified and morphological purity was calculated as the proportion of organoids showing the same morphology as the parental organoid post splitting.

### Outgrowth efficiency

Single cystic or budding organoids from lines at an early or late passage were manually picked and split. The efficiency was then quantified as the proportion of organoids formed post splitting of a single budding or cystic organoid.

### Differentiation of hfPOs

hfPOs were cultured for 14–21 days following passaging prior to being subjected to differentiation. hfPOs were washed with AdvDMEM+++ three times prior to adding differentiation medium.

The endocrine differentiation medium (hfPO-EC medium) was based upon previously published (i)PSC beta cell differentiation protocols<sup>110,111</sup> and contained advDMEM/F12 +++ supplemented with 1% Chemically Defined Lipid Concentrate (Thermo Fisher scientific), 1% B27 without Vitamin A (Thermo Fisher scientific), 50 µg/mL Vitamin C (Sigma Aldrich, #A92902), 2% KnockOut Serum Replacement (Thermo Fisher scientific), 10 µg/mL Heparin (Sigma-Aldrich), 10 µM Alk5 inhibitor (SCBT, sc-221234B), 20 ng/mL EGF (PeproTech), 0.1 µM Retinoic Acid (Sigma-Aldrich), 0.25 µM SANT1 (SCBT, sc-203253), 1 µM 3,3',5-Triiodo-L-thyronine sodium salt (T3) (Sigma-Aldrich) and 1 µM Gamma secretase Inhibitor II (LY411575, Sigma-Aldrich). For differentiation towards the acinar lineage, the medium was further supplemented with 200 nM dexamethasone (Sigma-Aldrich).

### Cell type quantification

To calculate how often an organoid was positive for a specific marker, 150–200 organoids were used. An organoid was scored as positive as long as it had > 0 marker positive cells. Total number of marker positive organoids was then divided by the total number of organoids.

To calculate the percentage of marker positive cells within an organoid the total number of cells per organoid quantified (ImageJ cell counter function). Subsequently, the number of the different cell types in the same organoid was quantified and the proportion of positive cells calculated. Unless otherwise stated, a minimum of 2 biological replicates with 10–12 technical replicates/ biological replicate was used for each condition.

### Enzyme activity sample collection and assays

To collect samples for ELISA and enzyme activity assays organoids were first cultured in expansion or differentiation medium. Organoids were released from their Matrigel domes using dispase (20ug/ml) and incubation for 15min. Organoids were washed five times with PBSO and then incubated for 2h in PBSO with 10uM FSK and 10uM IBMX.

Organoid supernatants were collected and centrifuged at max speed for 2min to remove any debris. Supernatants were frozen and stored at -80 degrees until used. ELISA and enzyme activity assays were performed according to the manufacturer's instructions.

### CRISPR organoid reporter-line generation

Spacer sequences targeting the genes CHGA, CPA1 and PTF1A were obtained from the resource provided by Schmid-Burgk et al.<sup>51</sup> and cloned into an empty sgRNA plasmid backbone (Addgene plasmid #65777) using inverse PCR (Q5 polymerase, NEB). Individual plasmids were sequenced to confirm correct sequence using Sanger sequencing (Macrogen). All primer sequences for sgRNA generation can be found in Table S6.

The electroporation protocol was adapted from Fujii et al.<sup>112</sup> In brief, one day prior to electroporation hfPO medium containing 1.25% (v/v) DMSO was added to the organoids. On the day of electroporation, organoids were removed from the Matrigel by washing two times with ice cold advDMEM/F12 +++. Organoids were then incubated in TrypLE for 3 minutes at 37°C, mechanically dissociated into single cells/small fragments by pipetting and washed two times in ice cold Optimem (Sigma) supplemented with Y-27632 (10 µM). The cell pellet was resuspended in 100 µL Optimem combined with the DNA mixture (total of max 20 µg). Following electroporation, the cells were transferred to eppendorf tubes and left to recover in complete medium at room temperature for 20 min. They were then spun down and resuspended in 300 µL Matrigel (80% Matrigel, 20% expansion media) and plated out in 40 µL per well of a pre-warmed 48-well tissue culture plate (Greiner). Selection with Blasticidin (InvivoGen) started once small round organoids had formed, typically 5–7 days post electroporation.

### Establishment of clonal lines, DNA extraction and Genotyping of Genetically Engineered Organoids

Post selection blasticidin resistant organoids were manually picked under a bright field microscope and expanded as clonal lines. 2–3 weeks post passaging a few organoids were collected from each line and used for DNA extraction (Quick-DNA microprep kit, Zymo research) following the manufacturer's instructions. Extracted DNA was used as template for PCR amplification of the target region (junction between the genomic DNA of the C-terminus of the gene of interest and the fluorescent reporter) by Q5 high fidelity polymerase (NEB). 5µl of the PCR products were loaded on a 1% UltraPure agarose gel (ThermoFisher). PCR products for which a single band could be observed were subjected to QIAquick PCR purification (Qiagen) according to the manufacturer's instructions. For PCR products for which multiple bands were observed, the band showing the predicted size was manually cut out and DNA extracted using the QIAquick gel extraction kit (Qiagen). Finally, PCR products were sent for Sanger sequencing (Macrogen) with the forward, reverse or sequencing primers. All genotyping primers can be found in Table S4. Sequencing results were analysed *in silico* using Benchling (<https://www.benchling.com/>).

### Immunohistochemistry (IHC)

Organoids were harvested and incubated in Cell Recovery solution (Corning, Product No. 354253) for 30 min on ice to remove all Matrigel. Organoids were then washed two times with pre-chilled PBS without calcium and magnesium before being transferred to glass vials and incubated in formalin (Sigma) for 30 min at room temperature. Organoids were subsequently dehydrated, paraffin embedded, and sectioned. Standard H&E stainings were performed as well as immunohistochemistry using antibodies against Chromogranin A (Thermo Scientific, clone: LK2H10) dilution 1:1000. Images were acquired using the VS200 slidescanner (Olympus). All antibodies used can be found in [key resources table](#).

### Immunofluorescence (IF) and confocal microscopy

Organoids were prepared for whole mount immunofluorescence as previously described in Pleguezuelos-Manzano et al.<sup>113</sup> Images were acquired using the Zeiss LSM900 confocal microscope and images were processed using the Zen Black software. All antibodies used can be found in [key resources table](#).

### Transmission electron microscopy (TEM)

Organoids were chemically fixed in 1.5% glutaraldehyde in 0.067 M cacodylate buffered to pH 7.4 and 1% sucrose for 12h at 4 °C. Following a single wash in 0.1 M cacodylate (pH 7.4), 1% sucrose and 3x with 0.1 M cacodylate (pH 7.4), organoids were incubated in 1% osmium tetroxide and 1.5% K<sub>4</sub>Fe(CN)<sub>6</sub> in 0.1 M sodium cacodylate (pH 7.4) for 1 h at 4 °C. Next organoids were dehydrated in ethanol (70%, 90%, up to 100%) infiltrated with Epon resin for 2 days, and finally embedded in the same resin and polymerized at 60 °C for 48 h. Ultrathin sections were cut on a Leica Ultracut UCT ultramicrotome (Leica Microsystems) using a diamond knife (Diatome), and mounted on Formvar-coated copper grids. Subsequent staining of the sections with 2% uranyl acetate in 50% ethanol and lead citrate allowed visualisation under a Tecnai T12 Electron Microscope equipped with an Eagle 4k × 4k CCD camera (Thermo Fisher). Images were stitched, uploaded, shared and annotated using Omero and PathViewer.

### CryoEM immunogold

For immunolabeling, organoids were chemically fixed with 4% paraformaldehyde in 0.1 M phosphate buffer. After washing with 0.1 M phosphate buffer, organoids were embedded in 12% gelatin and infused in 2.3 M sucrose for 24 hours. Mounted gelatin blocks were frozen in liquid nitrogen. Thin sections were prepared in a cryo ultramicrotome (Leica EM Ultracut UC6/FC6, Leica Microsystems, Vienna, Austria). Ultrathin cryosections were collected with 2% methylcellulose in 2.3 M sucrose.

Cryosections were incubated on drops of PBS for 45 min at 37°C, followed by 50mM glycine in PBS for 10 min and 1% BSA in PBS for 15 min at room temperature. Then, they were incubated with rabbit anti-Carboxypeptidase A (1:10; Abcam ab173283) diluted in 1% BSA in PBS for 1 hour. After five washes on drops of 0.1% BSA in PBS for 10 min, sections were incubated for 20 min with protein-A coupled to 10 nm diameter colloidal gold particles (1:50; CMC Utrecht) diluted in 1% BSA in PBS. Sections were fixed with 1% glutaraldehyde in PBS for 5 min. This was followed by washes with drops of PBS for 15 min and two washes with distilled water. Grids were embedded in a thin layer of 1.8% methylcellulose (25 Ctp) containing 0.4% Uranyl acetate. As a control for non-specific binding of the colloidal gold-conjugated antibody, the primary antibody was omitted. Microscopy was carried out on an Electron Microscope Tecnai Spirit (Thermo Fisher Scientific Company, The Netherlands) with an Eagle 4kx4k CCD camera.

### RNA extraction, quantification and quality control

Organoids were collected and RNA isolated using the RNeasy Mini Kit (QIAGEN) following the manufacturer's instructions. RNA was resuspended in DNase and RNase free water (Sigma) and quantified with a Nanodrop (Thermo Fisher).

### RT-qPCR

RNA isolation was performed as previously described. We used 0.5–1 µg RNA reverse transcription with Oligo(dT)<sub>15</sub> Primer and Random Primer using GoScript Reverse Transcriptase kit (Promega). The cDNA was used for RT-qPCR using iQ SYBRGreen supermix (BioRad) and gene specific primers ([Table S6](#)) in CFX Connect Real-Time PCR machine (BioRad). The results were analysed by normalisation to the housekeeping gene ( $\Delta C_t$ ) and adult pancreatic tissue (Amsbio, 5 donor pool) using the  $2^{-\Delta\Delta C_t}$  method.

### Bulk RNA-seq analysis

Budding and cystic organoids were individually handpicked, RNA extracted and subjected to bulk RNA sequencing. RNA extraction was performed as described above and integrity was determined using the Agilent RNA 6000 Nano kit with the Agilent 2100 Bioanalyzer (Agilent). RNA integrity (RIN) values ranged from 9.0–10.0. Samples used for bulk RNA-sequencing did not have a RIN <9.0. RNA concentrations were determined using the Qubit RNA HS Assay Kit (Thermo Fisher). RNA libraries were prepared with the TruSeq Stranded messenger RNA polyA kit and paired-end (2 × 50 base pairs) sequenced on an Illumina NextSeq 2000. Reads were mapped to the human GRCh38 genome assembly using STAR.<sup>114</sup> Differential gene expression analysis was performed using the DESeq2<sup>105</sup> package in RStudio (v.2022.02.2). Log<sub>2</sub> fold changes (FC) and significance (P values, Wald test) are indicated throughout the paper. Data visualization was performed using the packages ggplot2, ComplexHeatmap and EnhancedVolcano in RStudio, or manually plotted using GraphPad Prism (v.8.2.0). Software, packages and algorithms are listed in [key resources table](#).

### Flow cytometry and cell sorting

Organoids were incubated in 75% TrypLE (ThermoFisher) for 3min at 37°C and then dissociated into single cells by pipetting. Following two washes in advDMEM/F12 +++ the single cell suspension was filtered through the 35µm mesh of the FACS tube (Falcon). Cells were stained with DAPI for live/dead discrimination. FACS was performed on BD Fusion™ cell sorter (BD Bioscience) and data were analysed in FlowJo (Tree Star) or R.

### Single-cell derived clonal organoid lines

Organoids were dissociated to single cells using enzymatic digestion (TrypLE, for 3-5min at 37°C), washed three times with advDMEM/F12 +++ and filtered through the 35µm mesh of the FACS tube (Falcon). Cells were stained with DAPI for live/dead discrimination. FACS was performed on BD Fusion™ cell sorter (BD Bioscience). FACS sorted single cells were diluted to a concentration of 0.5 cells per 20ul Matrigel. Droplets of 20ul Matrigel were seeded in pre-warmed tissue culture plates (Greiner) and hfPO expansion medium was added. Medium was refreshed every 3 days.

### Single-cell transcriptome sample preparation

For scRNA-seq cells were FACS sorted into 384-well plates pre-printed with primers (SCD) and stored at -80°C until used for library preparation. Libraries were prepared according to the previously published VASA-Seq protocol for VASA-plate<sup>62</sup> and sequenced on a NextSeq2000, high-output 100 cycles flowcell (Illumina) with the following parameters, Read1 26 cycles (index and UMI), Read2 75 cycles.

### scRNA-seq analysis

#### FASTQ file pre-processing and mapping of sequencing reads

FASTQ file pre-processing and mapping was performed as previously described in Salmen et al.<sup>62</sup> In short, Read1 contains a 6-nt UFI/UMI, followed by an 8nt cell-specific barcode. Each barcode corresponding to a well in a 384-well plate. Sequenced barcodes that could be uniquely assigned to one of the 384 barcodes with a Hamming distance of 1nt or less were merged.

For mapping, read2 was assigned to the barcodes extracted from read1. Trimming of Read2 was performed with TrimGalore (version 0.4.3) and homopolymer removal by cutadapt (version 2.10).<sup>115</sup> Using bwa mem and bwa aln (version 0.7.10)<sup>116</sup> the trimmed reads were mapped to human rRNA (National Center for Biotechnology Information) to perform in silico ribosomal depletion. Post filtering of multi- and single-mappers the remaining reads were mapped to human GRCh38 genome (Ensembl 99) using STAR.<sup>114</sup> Assignment of reads was done according to Salmen et al.<sup>62</sup>

#### scRNA-seq analysis of bulk hfPO and 10x tissue libraries

The Shendure dataset was downloaded from GEO (GSE156793, <https://www.ncbi.nlm.nih.gov/geo/query/acc.cgi?acc=GSE156793>),<sup>16</sup> the Tabula Sapiens dataset was downloaded from GEO (<https://www.ncbi.nlm.nih.gov/geo/query/acc.cgi?acc=GSE201333>)<sup>71</sup> and the Xu dataset from <https://bigd.big.ac.cn/omix/> (identifier OMIX236).<sup>18</sup> Quality control (QC) was performed individually for each dataset. For the Xu and Shendure dataset only cells with >2000 transcripts, >200 genes, <170 000 transcripts, <20% mitochondrial reads were kept. For the Tabula Sapiens dataset only cells with >1200 transcripts, >200 genes, <170 000 transcripts, <18% mitochondrial reads were kept. Genes present in < 3 cells were excluded. In addition, Scrublet<sup>117</sup> was used to remove doublets. For the bulk hfPO dataset cells with > 20000 transcripts, <175 000 transcripts, <5% mitochondrial reads and a minimum of 3000 genes were kept. Genes present in < 3 cells were excluded. Highly variable genes with mean log expression between 0.0125 and 3 were selected, and cell cycle genes were excluded. Number of counts and cell cycle properties were regressed out (Scanpy function scanpy.pp.regress.out). Next, tissue datasets were filtered to keep only EPCAM<sup>+</sup> cells. Gene names in all datasets were set to be the same for all dataset using custom-made code. Next, the post-QC expression matrices were merged using anndata<sup>118</sup> and Scanpy<sup>106</sup> and custom-made code was used for further analysis. We performed principal component analysis (PCA), selecting 40 components and generated a 2D dimensional reduction using uniform manifold approximation and projection (UMAP).<sup>119</sup> Data integration of the datasets containing cells from tissue and organoids was performed using Harmony.<sup>120</sup> Integration of the datasets containing all time points was done on the factors dataset and system, and for the dataset containing selected time points on the factors dataset, system and plate. Unsupervised hierarchical clustering was done using the Leiden algorithm<sup>121</sup> (scanpy.tl.leiden) and finally differential gene expression between the clusters was calculated using t-test (default scanpy.tl.rank\_genes\_groups).

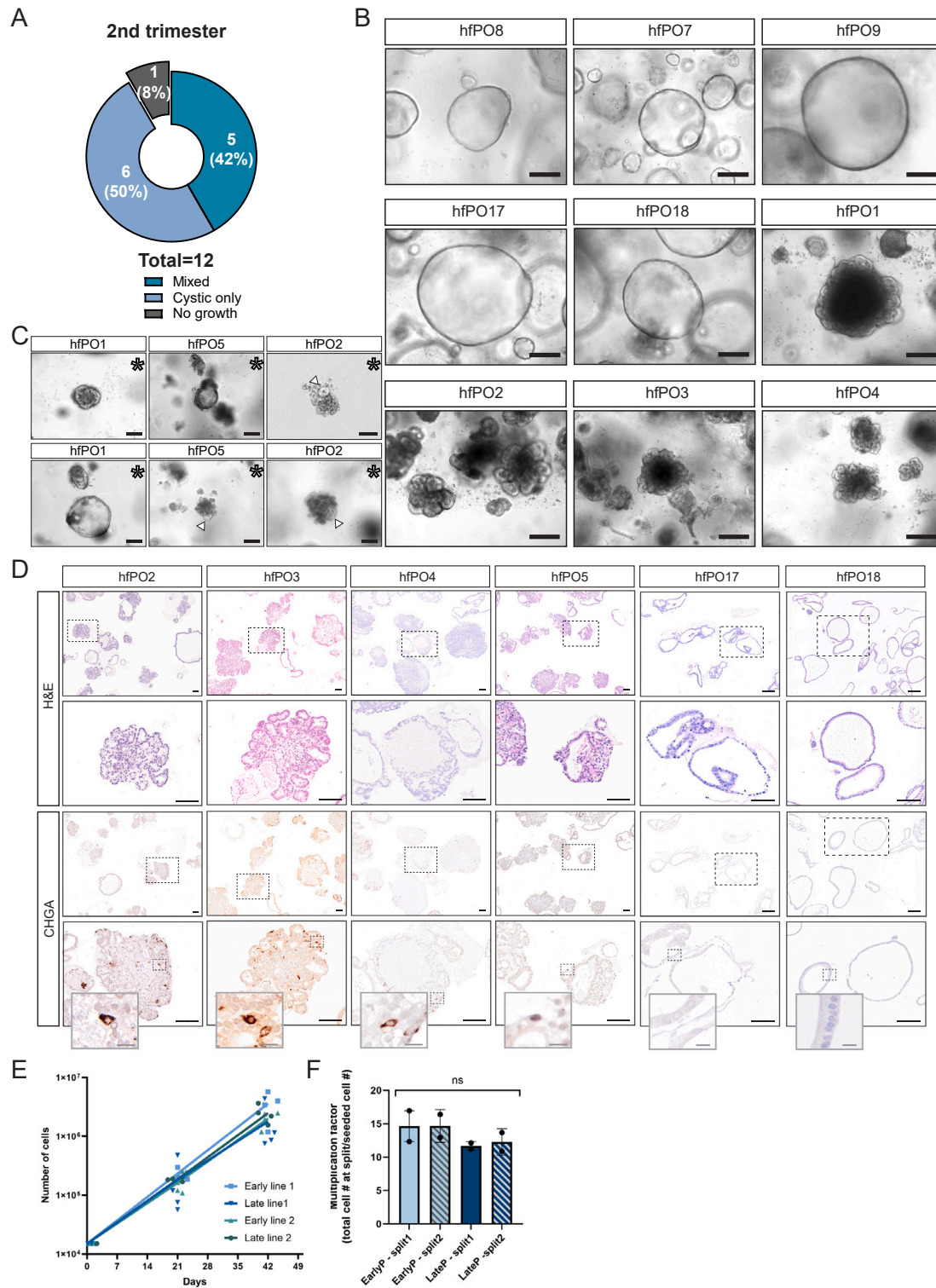
#### scRNA-seq analysis of single cell-derived hfPO libraries

For the single cell-derived hfPO dataset cells with > 20000 transcripts, <175 000 transcripts, <5% mitochondrial reads and a minimum of 3000 genes were kept. Genes present < 3 cells were excluded. Highly variable genes with mean log expression between 0.0125 and 3 were selected, and cell cycle genes were excluded. Number of counts and cell cycle properties were regressed out (Scanpy function scanpy.pp.regress.out). We selected the top 30 PCs and dimensional reduction was done using UMAP. For the dataset containing only clonal organoids integration was performed using Scanorama<sup>122</sup> and integrated on the factor plate. Clustering was performed using the supervised hierarchical Leiden algorithm<sup>121</sup> (scanpy.tl.leiden) and finally differential gene expression between the clusters was calculated using t-test (default scanpy.tl.rank\_genes\_groups). Software and packages are listed in the [key resources table](#).

### QUANTIFICATION AND STATISTICAL ANALYSIS

No statistical methods were used to predetermine sample size. The experiments were not randomized, and the investigators were not blinded to sample allocation during experiments and outcome assessment. Statistical analyses were performed in GraphPad Prism using t-test, one- or two-way ANOVA. For data derived from bulk RNA-Seq Wald test, as part of the DESeq2 pipeline, was used. For scRNA-Seq data Wilcoxon, as part of the scanpy pipeline was used. All experiments, except for the scRNA-Seq, in this manuscript have been reproduced with similar results using at least two independent organoid lines and performed as at least three independent experiments. The number of times the experiments were repeated with independently-derived organoid lines (n numbers), statistical tests, P values and considered statistical significance are reported in the figure legends.

# Supplemental figures



(legend on next page)

---

**Figure S1. Establishment of a hfPO biobank, related to Figure 1 and Table S1**

(A) Pie chart showing the success rate and morphology of hfPO lines established from the 2nd trimester.

(B) Representative bright-field images of cystic and budding hfPO lines.

(C) Representative bright-field images of 3 different hfPO lines 3 days post thawing, after 2.5 years in  $-80^{\circ}$ .

(D) Representative histology H&E and immunostaining against CHGA images of hfPO lines.

(E) Growth rate in number of cells over two passages of two individual organoid lines from early (p10) and late (p25) passages.

(F) Multiplication factor (increase in cell number) between passages of two individual organoid lines from early (p10) and late (p25) passages. Line 1, hfPO1; line 2, hfPO2 for (E) and (F). Technical triplicates were used for each line. Scale bars, 200  $\mu\text{m}$  (B); 100  $\mu\text{m}$  for all lines but hfPO2 (top right); 25  $\mu\text{m}$  (C); and 100 and 10  $\mu\text{m}$  for inserts (D).

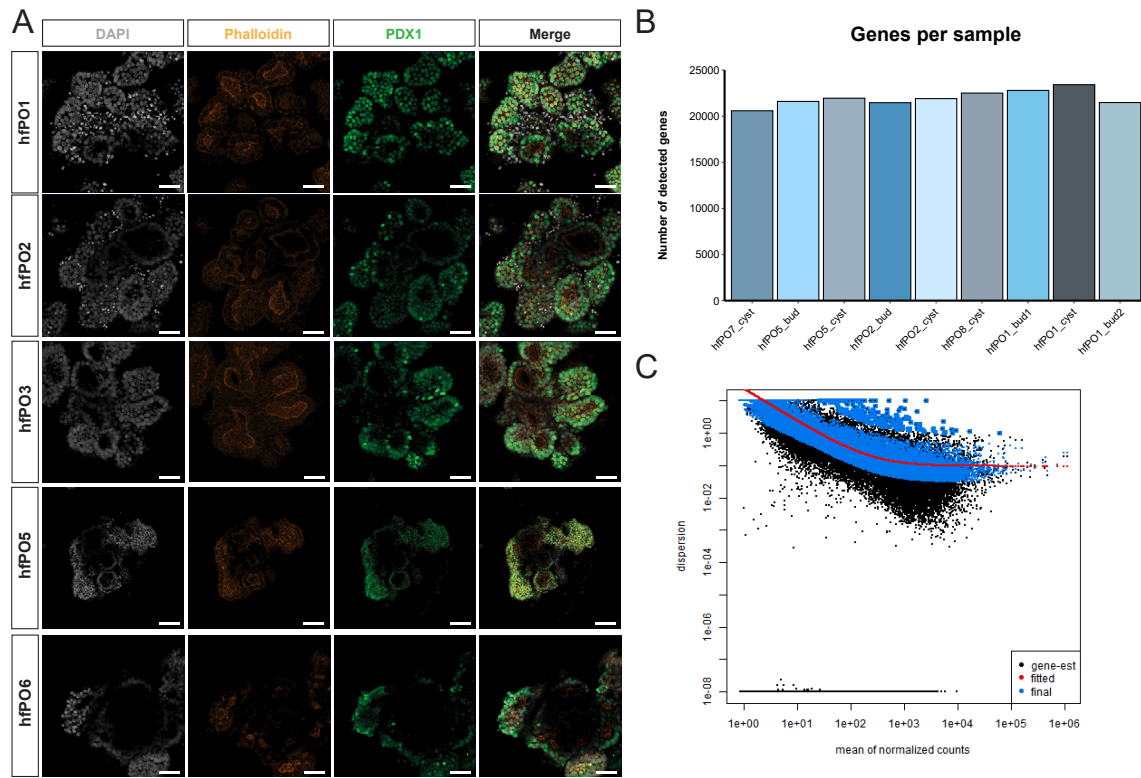
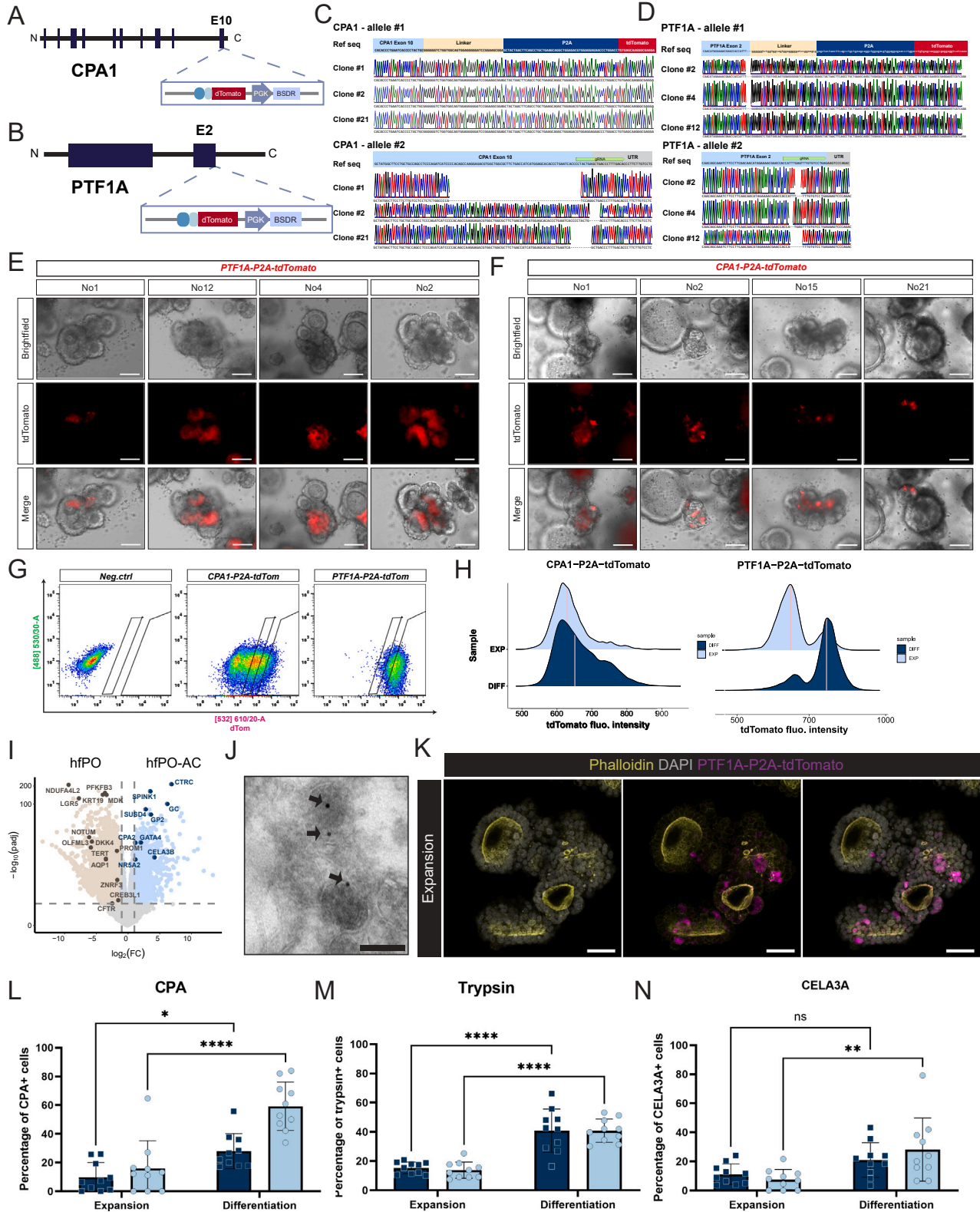


**Figure S2. Bulk RNA-seq analysis of cystic and budding hfPOs, related to Figure 2**

(A) Representative confocal images of hfPO lines stained for DAPI, phalloidin, and PDX1. Scale bars, 50  $\mu$ m (experiment repeated 3 times for each line).

(B) Bar graph showing the number of genes for the samples used for bulk sequencing.

(C) Quality control dispersion plot generated using the DESeq2 pipeline.



(legend on next page)

**Figure S3. Generation of acinar cell reporter organoid lines, related to Figure 3**

(A and B) Schematic images showing the insertion site for the reporter construct at the C-terminal end of CPA1 (top) and PTF1A (bottom).  
 (C and D) Sanger sequencing traces of allele 1 and allele 2 of 3 different CPA1 (B) and PTF1A (C) reporter hfPO lines.  
 (E and F) Bright-field and fluorescent images of 4 different hfPO CPA1 and PTF1A clonal reporter lines. Scale bars, 100  $\mu\text{m}$ .  
 (G) Gating strategy used for flow cytometric analysis of single, tdTomato-positive live cells from hfPO CPA1 and PTF1A reporter lines.  
 (H) Ridge plots showing the expression of CPA1 and PTF1A as measured by tdTomato fluorescence and quantification of negative (Neg), medium (Low), or high (High) expression of the reporter. PTF1A reporter generated in hfPO1 and hfPO2, experiment repeated twice, two clones from each line. CPA1 reporter generated in hfPO2, experiment repeated for 3 reporter clones, and for two clones, the experiment was performed twice.  
 (I) Volcano plot showing the transcriptional changes between hfPOs cultured in hfPO- and hfPO-AC medium. The  $\log_2$  fold change in is represented on the x axis and the  $-\log_{10}$  adjusted  $p$  value on the y axis. A  $p$  value of 0.05 and a fold change of 2 are indicated by gray lines.  
 (J) Cryoelectron microscopy (cryo-EM) immunogold against carboxypeptidase A (CPA). Arrows pointing at immunogold particles.  
 (K) Confocal images of PTF1A reporter-positive organoids (representative images from  $n = 2$  different lines, 3 different clones per line). Scale bars, 50  $\mu\text{m}$ .  
 (L–N) Quantification of the percentage of CPA<sup>+</sup> (L), trypsin<sup>+</sup> (M), and CELA3A<sup>+</sup> cells (N) in expansion and differentiation medium. For each condition (expansion, hfPO; differentiation, hfPO-EC), we used 2 different organoid lines. For quantification of how often the markers appeared in all organoids 2–4 images were used to reach 150–200 organoids. For quantification of the % of marker-positive cells among all cells within an organoid (proportions), 10 organoids (technical replicates) were used. Data are represented as mean  $\pm$  SD. For (L), \* $p < 0.05$ , \*\* $p < 0.0001$ . For (M), \*\*\*\* $p < 0.0001$ . For (N), \*\* $p < 0.0075$ . Scale bars, 200  $\mu\text{m}$  (E and F) and 125 nm (J), and 50  $\mu\text{m}$  (K).



---

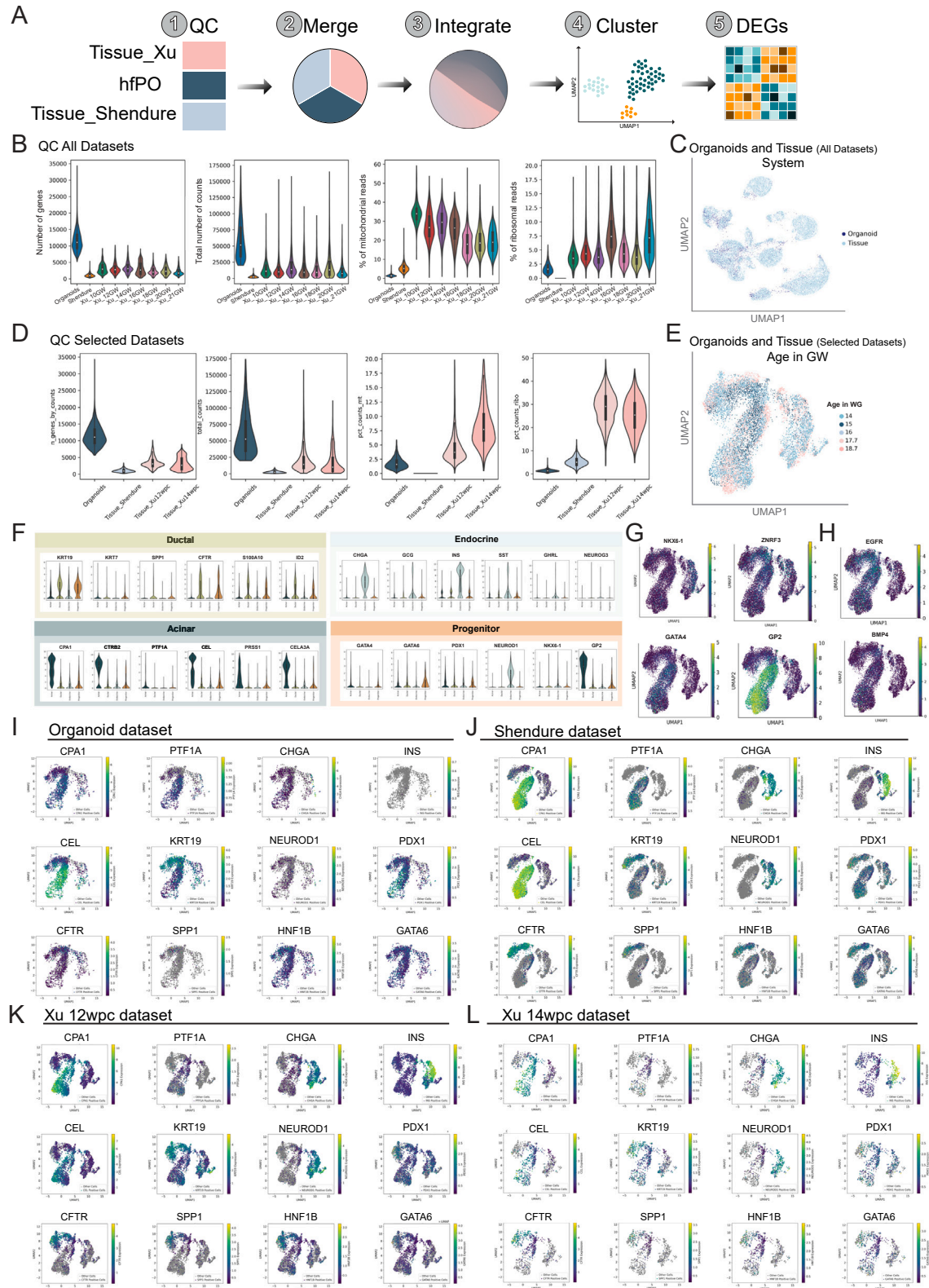
(C) Quality control dispersion plot generated using the DESeq2 pipeline and bar graph showing the number of genes for the samples used for bulk sequencing ( $n = 5$  different clones from the PTF1A hfPO1 line cultured in hfPO medium) differentiation ( $n = 3$  different clones from the PTF1A reporter hfPO1 line cultured in hfPO-AC medium).

(D) Bar graph showing the number of genes for the samples used for bulk sequencing.

(E) Gene set enrichment analysis (GSEA) of hfPO organoids cultured in hfPO vs. hfPO-EC medium as compared with the list of MSigDB and GO pathways. For the bulk-seq analysis (C–E), the lines 3 different hfPO1 CHGA reporter clones were used cultured in either hfPO medium or hfPO-EC medium.

(F) Representative TEM images of hfPO lines following 10 days in hfPO-EC medium.

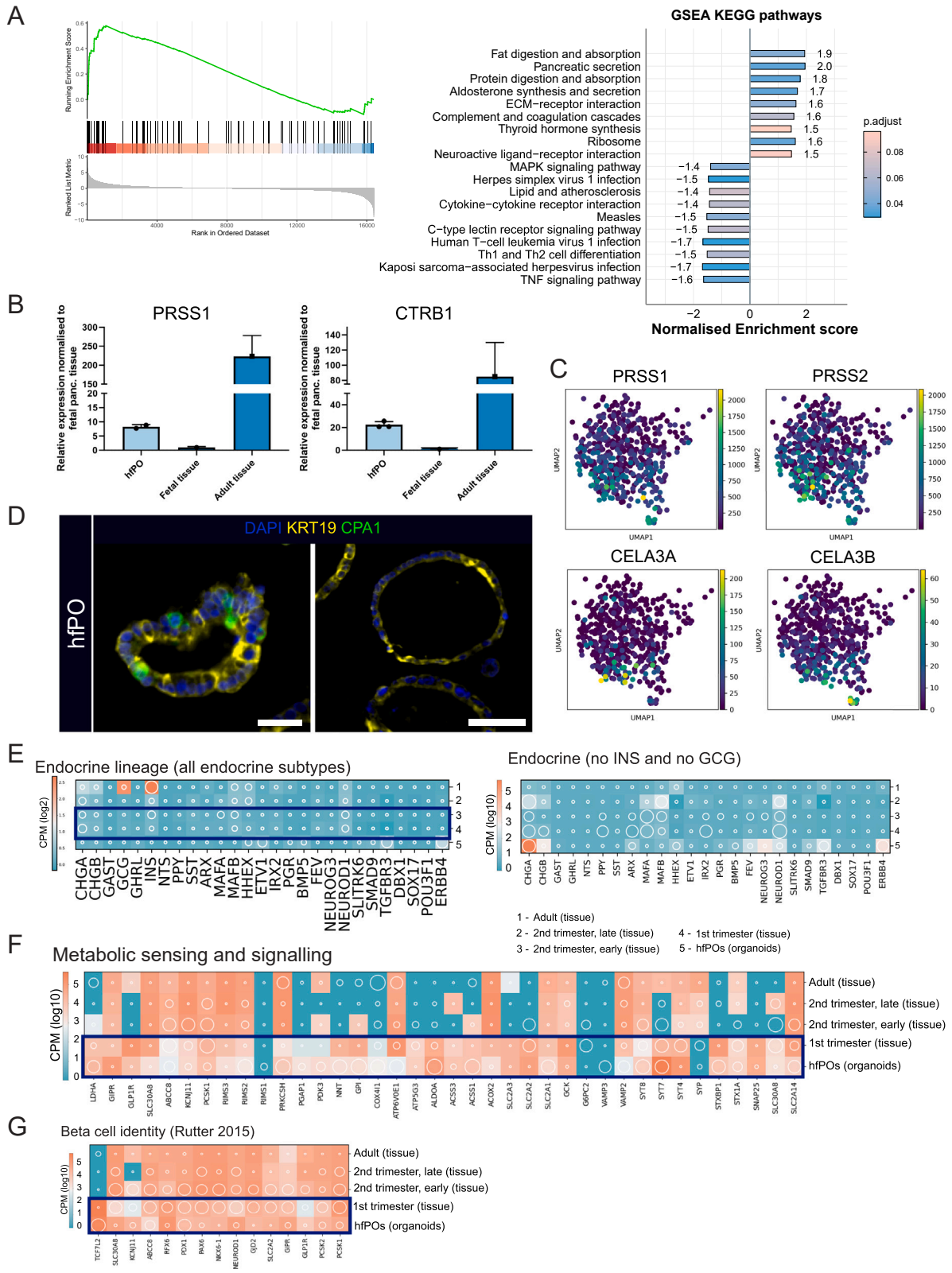
(G–L) Quantification of MKI67<sup>+</sup> (G), MUC1<sup>+</sup> (I), and CHGA<sup>+</sup> hfPOs (K) and the number of MKI67<sup>+</sup> (H), MUC1<sup>+</sup> (I), and CHGA<sup>+</sup> (J) cells within an hfPO (L). Two different biological replicates (hfPO lines 1 and 2) and at least ten technical replicates. Data are represented as mean  $\pm$  SD. \* $p < 0.025$ , \*\* $p < 0.0035$ , \*\*\*\* $p < 0.0001$ . Scale bars, 100 and 50  $\mu\text{m}$  (E) and 50  $\mu\text{m}$  (F).



---

**Figure S5. hfPOs recapitulate human fetal tissue at single-cell transcriptome level, related to Figure 5**

- (A) Schematic showing the scRNA-seq analysis pipeline. QC, quality control; DEGs, differentially expressed genes.
- (B) Quality control plots showing the number of genes, total number of counts, % of mitochondrial genes, and % of ribosomal genes.
- (C) UMAP visualization of the merged scRNA-seq dataset containing tissue samples of all different ages (in GW) from the Xu dataset.
- (D) Quality control plots showing the number of genes, total number of counts, % of mitochondrial genes, and % of ribosomal genes from the hfPO dataset and the "Xu tissue datasets." These datasets were selected based on their age being closest to the age of the tissue from which the hfPO was established.
- (E) UMAP plots visualizing the expression of genes of the acinar, ductal, endocrine, and progenitor cluster.
- (F) Violin plots showing the expression of marker genes related to the progenitor cluster.
- (G) Feature plots showing the expression of marker genes related to the progenitor cluster or literature.
- (H) Feature plots showing the expression of the growth factor BMP4 and growth factor receptor EGFR.
- (I–L) Feature plots showing the expression of the indicated markers for the individual datasets, hfPO organoid dataset (I), Shendure (J), Xu 12wpc (K), and Xu 14wpc (L).



---

**Figure S6. hfPOs recapitulate human fetal pancreatic tissue, related to Figure 6**

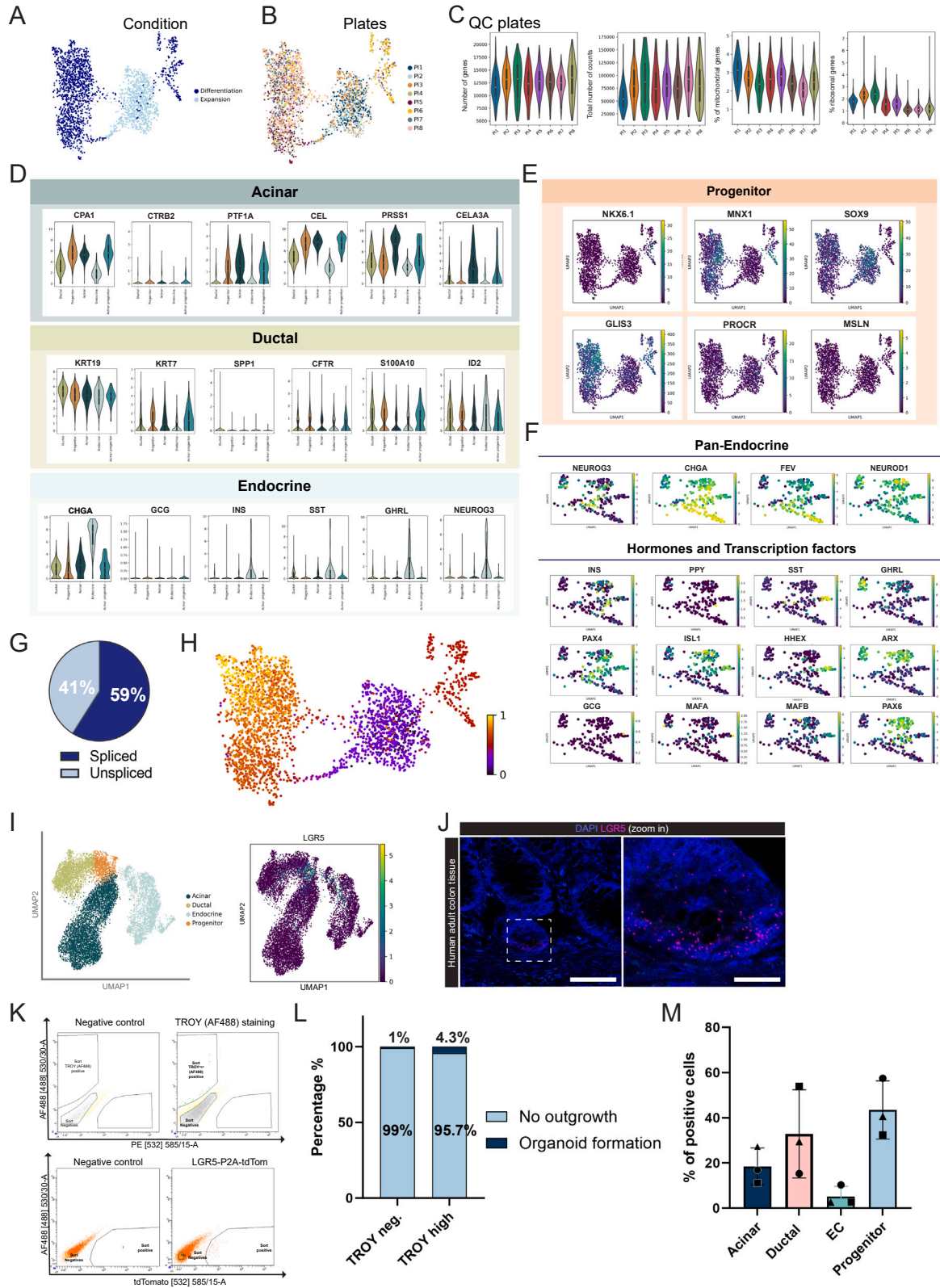
(A) GSEA enrichment analysis of hfPO organoids cultured in hfPO-AC vs. hfPO medium as compared with the list of Kyoto Encyclopedia of Genes and Genomes (KEGG) pathways. Enrichment of upregulated genes belonged to functions such as fat digestion and absorption as well as pancreatic secretion.

(B) RT-qPCR comparing the expression of the digestive enzymes PRSS1 and CTRB1 between hfPOs and fetal and adult tissue. Data are represented as mean  $\pm$  SD.

(C) UMAP plots visualizing the expression of the digestive enzymes PRSS1/2 and CELA3A/B from the hfPO scRNA-seq dataset.

(D) Representative confocal images of cystic organoids stained for KRT19 and CPA1. Scale bars, 25  $\mu$ m.

(E–G) Expression profiles for key marker genes for the (E) endocrine cell lineage, right plot with the presence of insulin and glucagon and the left plot without INS and GCG, to allow assessment of the expression of the other hormones (F) Metabolic sensing and signaling for  $\beta$  cells, and (G) marker genes of beta cell identity function. Shading displays mean expression (CPM, log scaled), and diameter denotes fractional expression.

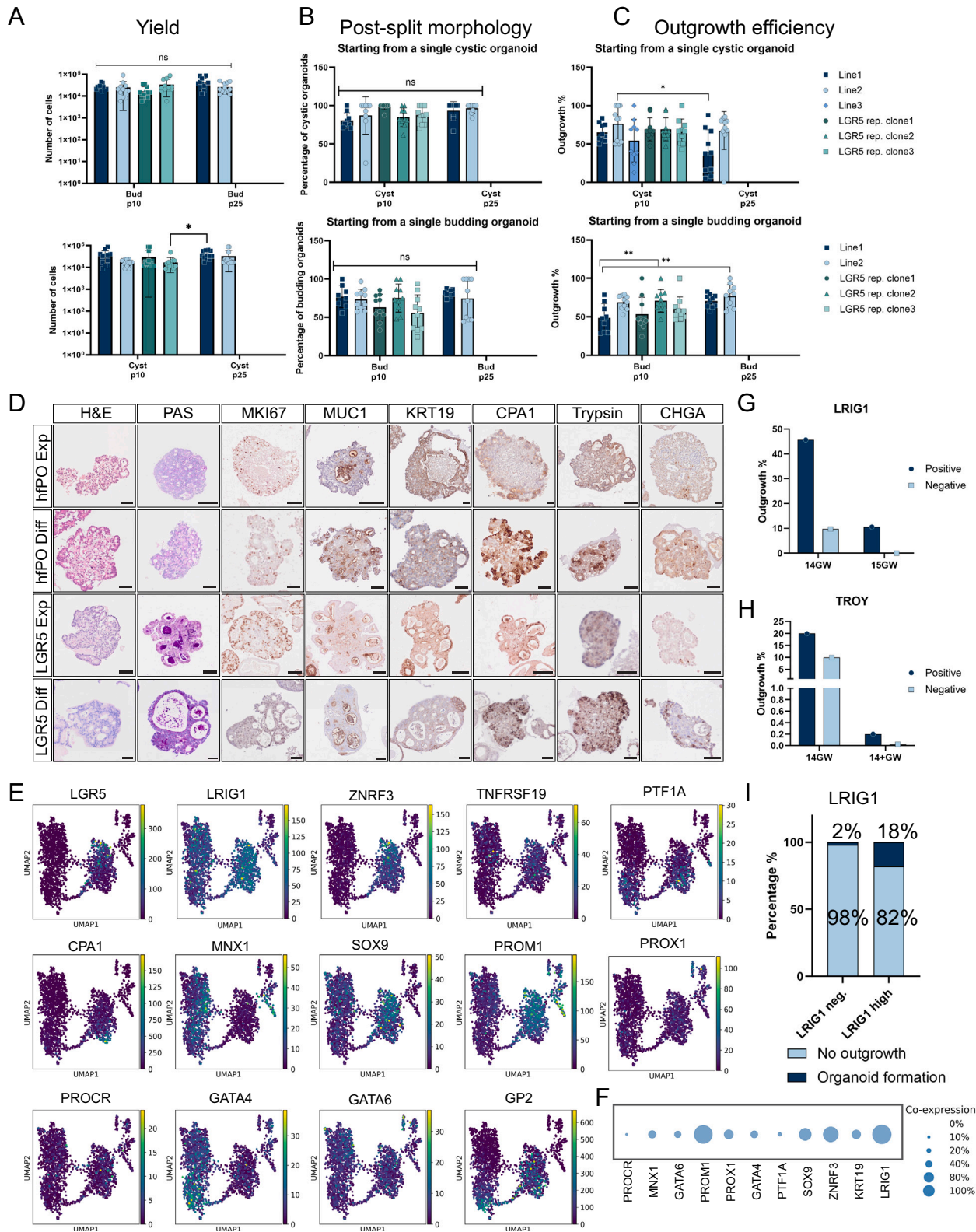


(legend on next page)

---

**Figure S7. LGR5 marks tripotent human pancreatic progenitors, related to Figure 7**

- (A) UMAP visualization of the culture conditions of the hfPOs.
- (B) UMAP visualization of the different plates.
- (C) Quality control plots showing the number of genes, total number of counts, % of mitochondrial genes, and % of ribosomal genes.
- (D) Feature plots showing the expression of marker genes characterizing the acinar, ductal, and endocrine cluster.
- (E) Feature plots of marker genes used to define the progenitor cluster.
- (F) Feature plots of subclustered endocrine cells showing the expression of pan-endocrine factors and hormones and transcription factors.
- (G) Fraction of spliced and unspliced transcripts in the VASA-seq dataset.
- (H) UMAP with unbiased scVelo pseudotime. 0 denotes starting time and 1 end time point.
- (I) UMAPs showing the clusters as well as the expression of LGR5.
- (J) Confocal images of human colon tissue stained for DAPI and RNAScope probe against LGR5. Scale bars, 100  $\mu$ m.
- (K) Representative FACS analysis plots of TROY and LGR5-sorted cells.
- (L) Bar graphs showing the outgrowth efficiency of TROY positive and negative cells.
- (M) Quantification of the proportion of the different cell lineages from whole-mount fluorescent hfPOs from 3 independent biological replicates (hfPO1, hfPO2, and hfPO4) and 5 technical replicates. Mean values from 5 technical replicates per line are shown.



(legend on next page)

---

**Figure S8. LGR5 stem cell analysis, related to Figure 7**

(A–C) The yield (A), post-split morphology (purity/post-split morphology) (B), and outgrowth efficiency (C) of LGR5-derived hfPOs were compared with that of hfPOs from fetal pancreas tissue for the early (p10) and late passage (p25) 2 biological replicates (line 1, hfPO1; line 2, hfPO2; line 3, hfPO4) and 10–12 technical replicates for each biological replicate. For the LGR5 reporter clones, p10 was the latest passage. Data are represented as mean  $\pm$  SD. \* $p < 0.045$ , \*\* $p < 0.0075$ .

(D) Morphology and expression of indicated marker genes of LGR5-derived hfPOs were compared with that of hfPOs from fetal pancreas tissue. Outgrowth efficiency of FACS-sorted LRIG1<sup>+</sup> and LRIG1<sup>-</sup> cells. Scale bars: hfPO Exp; H&E, 50  $\mu$ m, all others, 50  $\mu$ m, hfPO Diff; PAS, 100  $\mu$ m, MUC1, Trypsin, and CHGA, 100  $\mu$ m, all other 50  $\mu$ m. LGR5 Exp; CHGA 25  $\mu$ m, all others 50  $\mu$ m. LGR5 Diff; all 50  $\mu$ m.

(E) Expression profiles of progenitor marker genes of hfPOs.

(F) Dot plot showing the co-expression percentage of indicated marker genes within the LGR5<sup>+</sup> cells.

(G and H) (G) TROY<sup>+</sup> and TROY<sup>-</sup> cells (H) cells from primary fetal pancreatic tissue.

(I) Outgrowth efficiency of FACS-sorted LRIG1<sup>+</sup> and LRIG1<sup>-</sup> cells from hfPOs.